Structures of the heart specific SERCA2a Ca^{2+}-ATPase

Aljona Sitsel[1,2,3,4],Joren De Raeymaecker[5], Nikolaj Düring Drachmann[1,3], Rita Derua[2,6],Susanne Smaardijk[2], Jacob Lauwring Andersen[1,3,7], Ilse Vandecaetsbeek[2], Jialin Chen[2], Marc De Maeyer[5], Etienne Waelkens[2,6], Claus Olesen[3,7], Peter Vangheluwe[2,#], Poul Nissen[1,3,4,#]

1. Department of Molecular Biology and Genetics, Aarhus University, Aarhus 8000, Denmark
2. Department of Molecular Medicine, KU Leuven, Leuven 3000, Belgium
3. Center for Membrane Proteins in Cells and Disease – PUMPkin, Danish National Research Foundation
4. Danish Research Institute of Translational Neuroscience – DANDRITE, Nordic-EMBL Partnership for Molecular Medicine
5. Department of Chemistry, KU Leuven, B – 3000 Leuven, Belgium
6. SyBioMa, KU Leuven, Belgium
7. Department of Biomedicine, Aarhus University, DK – 8000 Aarhus C, Denmark

[#] Shared last and co-corresponding authors:

Poul Nissen
Gustav Wieds Vej 10C, Aarhus University
8000 Aarhus C, Denmark
Tel. +45 87 155 508
pn@mbg.au.dk

Peter Vangheluwe
Campus Gasthuisberg, ON1, KU Leuven
Herestraat 49, box 802
3000 Leuven, Belgium
Tel. +32 16 33 07 20
peter.vangheluwe@kuleuven.be

Running title

Comparison of SERCA muscle isoforms

Abbreviations: SERCA, Sarcoplasmic reticulum Ca^{2+}-ATPase; CPA, Cyclopiazonic acid; $C_{12}E_8$, octaethylene glycol monododecyl ether;

Author Contributions

Conceptualization, C.O., P.V., P.N.; Methodology, A.S., N.D., I.V., M.D.M., E.W., C.O., P.V., P.N.; Formal analysis, A.S., N.D., J.L.A., R.D., S.S.; Investigation, A.S., N.D., R.D., S.S., J.D.R., I.V., J.C.; Writing – original draft preparation, A.S., P.N., P.V.; Writing – review and editing, A.S., J.L.A., P.N., P.V.; Visualization, A.S. Supervision, C.O., P.V., P.N.; Funding acquisition, A.S., C.O., P.V., P.N.

Abstract

The isoform 2a of sarco/endoplasmic reticulum Ca^{2+}-ATPase (SERCA2a) performs active reuptake of cytoplasmic Ca^{2+} and is a major regulator of cardiac muscle contractility. Dysfunction or dysregulation of SERCA2a is associated with heart failure, while restoring its function is considered as a therapeutic strategy to restore cardiac performance, but its structure was not yet determined. Based on native, active protein purified from pig ventricular muscle, we present the first crystal structures of SERCA2a that were determined in the CPA-stabilized and H^+-occluded [$H_{2\text{-}3}$]E2-AlF_4 (3.3 Å) form, arranged as parallel dimers, and the Ca^{2+}-occluded [Ca_2]E1-ATP (4.0 Å) form. We compare these new structures to similar forms of the skeletal muscle SERCA1a and address structural, functional and regulatory differences. We show that the isoform specific motifs of SERCA2a allow a distinct regulation by post-translational modifications and affect the dynamic behavior, which may explain specific properties and regulation.

Keywords:

Ca^{2+} transport/Ca2+-ATPase/heart failure/Darier disease/crystal structure/molecular dynamics

Introduction

The cardiac contractility is tightly regulated by the activity of the sarco/endoplasmic reticulum Ca^{2+} ATPase 2a (SERCA2a), which is responsible for the re-uptake of cytosolic Ca^{2+} into the sarcoplasmic reticulum (SR) of cardiomyocytes. SERCA2a enables cardiac muscle relaxation and determines how much Ca^{2+} can be released for contraction, which in turn controls contractile strength (Bers, 2002). In the heart, the activity of SERCA2a is regulated by several transmembrane (TM) micropeptides: Phospholamban (PLB) (MacLennan & Kranias, 2003), Sarcolipin (SLN) (Vangheluwe *et al*, 2005), Dwarf Open Reading Frame (DWORF) (Nelson *et al*, 2016) and Another Regulin (ALN) (Anderson *et al*, 2016). These small TM proteins regulate SERCA2a activity mainly via controlling the apparent Ca^{2+} affinity of the pump within a narrow physiological range thereby allowing a dynamic regulation of cardiac contractility. For instance, in resting conditions PLB inhibits SERCA2a, which is temporally relieved during β-adrenergic stimulation, and exerts strong inotropic and lusitropic effects (Arkin *et al*, 1994).

A reduced SERCA2a activity at least in part contributes to the progressive deterioration of cardiac contractility in heart failure (HF). Lower SERCA2a expression (Periasamy *et al*, 2008) and protein sumoylation (Kho *et al*, 2011), together with reduced levels of DWORF (Nelson *et al*, 2016) and PLB phosphorylation (Periasamy *et al*, 2008), negatively impact on the uptake of Ca^{2+} into the SR, impairing the contractile performance of the heart. Also, some familial forms of dilated cardiomyopathy are caused by mutations in PLB, further highlighting the central role of SERCA2a dysregulation in HF (Trieber *et al*, 2005; Haghighi *et al*, 2003; Kimura *et al*, 1998). Conversely, restoring SERCA2a activity by elevating its expression or by PLB interference rescues contractility in isolated cardiomyocytes, and in small and large animal models (MacLennan & Kranias, 2003). Therefore, adeno-associated viral gene delivery of SERCA2a was explored in clinical trials as a therapeutic strategy for HF (Jessup *et al*, 2011; Hulot *et al*, 2017), although inadequate SERCA2a gene delivery has been noted (Greenberg *et al*, 2016). Alternative to gene delivery, small molecule SERCA2a agonists have been reported (Ferrandi *et al*, 2013; Kaneko *et al*, 2017), but molecular details of their working mechanism are lacking.

SERCA2a (encoded by the *ATP2A2* gene) is expressed in cardiac, smooth and slow-twitch skeletal muscles, while SERCA1a (*ATP2A1*) is the major isoform in fast-twitch skeletal muscles. Overall, they are similar and transport two Ca^{2+} ions per ATPase cycle. Based on numerous SERCA1a crystal structures capturing most conformational states along the functional cycle, the SERCA Ca^{2+} transport mechanism is well described at the functional and structural level (Bublitz *et al*, 2013; Winther *et al*, 2013; Toyoshima *et al*, 2013). Three cytoplasmic domains (*i.e.* the nucleotide binding domain, N; phosphorylation domain, P; and actuator domain, A) regulate ATP binding, autophosphorylation and

dephosphorylation, whereas a TM domain controls Ca^{2+} binding and translocation. During ion transport across the membrane, SERCA undergoes large conformational changes switching between Ca^{2+}-bound E1 states and Ca^{2+}-free E2 states (Moller *et al*, 2010; Post & Sen, 1965; Albers *et al*, 1963). In the E1 state, cytosolic Ca^{2+} enters via the Ca^{2+} entry gate and binds with high affinity at the TM domain. Mg^{2+}-ATP binds to the N-domain, resulting in the phosphorylation of an aspartate residue in the P domain (Asp351, conserved in all P-type ATPases) and the formation of an occluded [Ca_2]E1P intermediate. A spontaneous conformational transition to an E2P state, typically rate limiting for SERCA1a transport, opens the Ca^{2+} exit gate to the luminal compartment and allows Ca^{2+} release. Subsequently, negatively charged residues of the ion binding sites are partially protonated, which triggers occlusion and dephosphorylation, catalyzed by a conserved glutamate residue of the A domain (E183) via an E2-P_i intermediate (Olesen et al. 2004) and ending with the phosphate-released E2 state. The conversion of the protein to an E1 state opens the cytoplasmic Ca^{2+} entry gate, promoting the release of protons from the TM domain possibly via a C-terminal pathway (Bublitz *et al*, 2010) and allowing another cycle to begin (Winther *et al*, 2013; Toyoshima *et al*, 2013).

Compared to SERCA1a, heart muscle SERCA2a exhibits a lower maximal turnover rate and higher apparent Ca^{2+} affinity than SERCA1a (Dode *et al*, 2002, 2003). This implies that structural features somehow modify the kinetics of the Ca^{2+} transport mechanism. To study the SERCA2a specific properties, we purified porcine SERCA2a, which shares 99% sequence identity with the human SERCA2a and 84 % identity with rabbit and other mammalian SERCA1a. Subsequently, we determined structures of SERCA2a in a proton-occluded [H_{2-3}]E2-AlF_4^- complex stabilized by the SERCA inhibitor cyclopiazonic acid (CPA) and a Ca^{2+}-occluded E1 form using the non-hydrolyzable ATP analog AMPPCP. Furthermore, we compare SERCA1a and SERCA2a structures, and probe their regulation and dynamic behavior by molecular dynamics simulations, and address as well their functional differences using chimeric constructs.

Experimental Procedures

Isolation and purification of SERCA2a from pig heart

Pig hearts were collected from a slaughter house (Danish Crown in Horsens, Denmark) or obtained from the department of cardiovascular sciences (KU Leuven, Belgium), and were immediately rinsed with an ice-cold 0.9% (w/v) NaCl solution. All the following procedures were performed at 4°C. Ventricle tissue from the pig heart was homogenized with 10 mM $NaHCO_3$ buffer (1:3 w/w) and centrifuged for 20 min at 12,200 × g. The supernatant was filtered through eight layers of gauze and centrifuged as above. The filtering step was then repeated and the supernatant was centrifuged at 140,000 × g for 45 min. The pellet was re-suspended in buffer (0.6 M KCl, 10 mM histidine, pH 7.0), magnetically stirred for 30 min, and then centrifuged again at 140,000 × g for 45 min. The final pellet containing crude SR microsomes was re-suspended in a stabilizing buffer (8 mM $CaCl_2$, 50 mM MOPS-KOH, pH 7.0, 20% (vol/vol) added glycerol, 5 mM $MgCl_2$) and flash-frozen in liquid nitrogen. A similar protocol preparing for purification by Reactive Red 120 beads was published earlier (Yao *et al*, 1998). The protein was solubilized in n-Dodecyl β-D-Maltopyranoside (DDM) at a ratio of 1:3 (w/w). Once solubilized, the samples were centrifuged for 45 min at 200,000 × g at 4°C. The supernatant was loaded onto Reactive beads (Green Separophore 4B-CL, Bio-world) and incubated for 1 h. Beads were washed with 5 column volumes of wash buffer (20% (vol/vol) glycerol, 20 mM MOPS-KOH pH 7.0, 1 mM $CaCl_2$, 1 mg/ml $C_{12}E_8$; 0.35 mg/ml egg yolk phosphatidyl choline lipids (EYPC)). Finally, protein was eluted with 2 column volumes elution buffer (wash buffer with 50 mM NaCl and 4 mM AMPPCP). The protein concentration was measured using the Bradford protein assay (Bio-Rad). The presence of other SERCA isoforms was tested by Western Blot using the following antibodies: S2b AB (SERCA2b pAB serum, Badrilla); S2a AB (SERCA2a pAB serum, Badrilla) 1:100000; S2 AB (IID8) 1:2000.

Activity measurements of purified SERCA2a and COS1 microsomes

For the activity measurements, the wash and elution buffers for the protein purification contained 0.25 mg/ml $C_{12}E_8$ and no EYPC was added. The Ca^{2+}-dependent activity of the protein was measured using the Baginski assay probing inorganic phosphate released from ATPase activity (Baginski *et al*, 1967). Briefly, the reaction mixture containing 50 mM TES/TRIS, pH 6.9, 100 mM KCl, 7 mM $MgCl_2$, 1 mM ethylene glycol-bis(β-aminoethyl ether)-N,N,N',N'-tetraacetic acid (EGTA), 5 mM NaN_3, 0.2 mM $NaMoO_4$, 50 mM KNO_3, and 150 ng (purified enzyme) or 5 μg (COS1 microsomes) of the protein, as well as $CaCl_2$ in different concentrations was initiated with 5 mM ATP (final concentration) and incubated at 37°C for 20 min. The reaction was stopped with the double reaction volume of ascorbic acid solution (170 mM ascorbic acid dissolved 0.5 N HCl and mixed with 4 mM NH_4MoO_4, solutions kept on ice). The samples treated with ascorbic acid solutions were incubated for 5 minutes on ice, and then triple reaction volume of colorimetric solution (210 mM Na_3AsO_3, 155 mM sodium citrate and 58

mM acetic acid) was added to stabilize the color. The absorbance was measured at 850 nm wavelength after an additional 5 minutes incubation at 37°C. The results were analyzed in Excel and Origin (OriginLab Corporation).

Crystallization of SERCA2a

Purified SERCA2a was concentrated to 3.5 - 6 mg/ml and trace amounts of aggregated proteins pelleted by centrifugation at 100,000 × g for 10 min. Crystals were grown using the vapor-diffusion hanging-drop method, in which 1 µl of protein was mixed with 1 µl reservoir solution and equilibrated against 450 µl reservoir solution. For the CPA-stabilized E2-AlF_4 form, an egg yolk phosphatidylcholine (EYPC) to protein ratio of 1.7:1 (w/v) was used, and 200 μM CPA, 80 mM KCl, 15 mM $MgCl_2$, 2 mM EGTA and 10 mM NaF were added. The E2-AlF_4-CPA crystals were grown at 19^0 C for 4 days using reservoir solutions containing 14-20% PEG4000, 0-5% glycerol, 4-6% 2-Methyl-2,4-pentanediol and 100 mM Na^+ malonate in the reservoir and then stored at 4^0C. For the E1 conformation, the protein was treated with a final concentration of 10 mM $CaCl_2$, 80 mM KCl and 3 mM $MgCl_2$. [Ca_2]E1-AMPPCP crystals appeared with reservoir solutions containing 21% PEG2000 monomethyl ether, 20% glycerol, 100 mM NaCl, 5% *tert*-BuOH and 2.4% Zwittergent-3-08 and grew within 7-10 days at 19^0C. Crystals were fished with nylon loops. The E2-AlF_4-CPA crystals were swiftly dipped in a mixture of 1 μl reservoir solution and 1 μl of 50% glycerol for cryoprotection. The mounted crystals were flash cooled and stored in liquid nitrogen.

Data collection, processing and structural analysis

Diffraction data were collected at the Swiss Light Source (Villigen, Switzerland), at beam line PXI or PXII using a Pilatus 6M detector, with X-ray wavelengths at around 1 Å. Data were processed with XDS (Kabsch, 2010) to 3.3 Å maximum resolution in space group $P2_1$ for the E2-AlF_4-CPA form and to 4.0 Å in space group P2 for the [Ca_2]E1-AMPPCP form. The structures were determined by molecular replacement using PHASER-MR (McCoy *et al*, 2007) and SERCA1a as a search model (PDB entries 3FGO and 3N8G) and revealing in both cases one SERCA2a molecule in the asymmetric unit. Model building was performed in COOT (Emsley & Cowtan, 2004) using electron density maps calculated using PHENIX (Adams *et al*, 2010). Refinement of the structural model was done in PHENIX (Adams *et al*, 2010). Both structures were built using the iMDff technique (Croll & Andersen, 2016; Focht *et al*, 2017). Structures were analysed with Molprobity, indicating for the E2-AlF_4-CPA structure 98% residues in favored, 2% in further allowed, and 0 in non-favored region, with less than 1% rotamer outliers, and for the [Ca_2]E1-AMPPCP structure 96% residues in favored, 4% in further allowed and 0 in non-favored regions of the Ramachandran plot, with no outlier rotamers. Figures were prepared and further model analysis performed with PyMol. The root mean square deviation for Cα atoms between the SERCA2a and the corresponding SERCA1a structures were determined by the 'super' command in PyMol.

Molecular dynamics

Molecular Dynamics (MD) simulations were performed using the Gromacs package (version 4.5.3) (Hess *et al*, 2008). Each structure was placed in a dodecahedral box (x: 9.483 nm, y: 9.542 nm, z: 17.07 nm) and the system was solvated with TIP3P water molecules (Jorgensen *et al*, 1983). Lengths of x and y axis were fitted to the membrane dimensions. The energy of the system was minimized with 50,000 steps of steepest descent. Pre-equilibrated 1,2-Dioleoyl-sn-glycero-3-phosphocholine (DOPC) membrane structure and parameters were obtained from the Lipidbook website. The membrane system was energy minimized with 50,000 steps of steepest descent. Subsequently, all water molecules in the protein and membrane system were removed before merging them and inserting the protein into the membrane using g_membed tool in Gromacs. Next, the protein-membrane system was solvated with TIP3P and counter ions were added to neutralize the intrinsic negative charge of the SERCA2a structure. The energy of the protein-membrane system was minimized once more with 50,000 steps of steepest descent. The system was equilibrated using 500 ps of NVT ensemble with the V-rescale thermostat followed by 2 ns of NPT ensemble with the V-rescale thermostat and the Parrinello/Rahman barostat. Protein atoms and phosphorus atoms of lipid molecules were position restrained during equilibration with a force of 1000 kJ mol-1 nm-2. After equilibrium was reached, a full production MD without position restraint was performed for a time scale of 50 ns. In all simulations, an all atom AMBER99SB force field supplemented with AMBER-GAFF force field parameters for DOPC membrane (available on Lipidbook website) was employed.

Plasmids, mutagenesis and cell culture

SERCA1a in pcDNA3.1 and SERCA2a in pMT2 were used for all expression experiments (Dode *et al*, 2003). Mutants were generated using the Quickchange site-directed mutagenesis kit (StrataGene) or the Q5 mutagenesis kit (New England Biolabs). A SERCA1a chimera with the luminal loop connecting transmembrane segments 7 and 8 (L7/8) of SERCA2a was previously described (Clausen *et al*, 2012). The reverse SERCA2a chimera with L7/8 of SERCA1a was generated using BBVC1 and BMGB1 restriction sites. Transfection into COS1 cells was performed with GeneJuice transfection reagent (Invitrogen). 72 h after transfection, the microsomal fraction was isolated by differential centrifugation as described previously (Maruyama & MacLennan, 1988).

Mass Spectrometry

SERCA1a was purified according to a previously published protocol (Young *et al*, 1997). 10 μg of purified SERCA2a and SERCA1a were reduced by 5 mM DTT and alkylated with 25 mM iodoacetamide, followed by precipitation (Wessel and Flügge 1984). The proteins were digested overnight using 0.5 μg trypsin at 37ºC in 200 mM ammonium bicarbonate, 5% acetonitrile, 0.01 % ProteaseMax (Promega). The resulting peptides were desalted with C18 ZipTip pipette tips (Millipore),

and high-resolution LC-MS/MS on a 15 cm EASY-spray C18 column (Thermo Fisher Scientific) was performed using an Ultimate 3000 nano UPLC system interfaced with a Q Exactive hybrid quadrupole-orbitrap mass spectrometer. Peptides were identified by MASCOT (Matrix Science) using the SwissProt mammalian database via the Proteome Discoverer 2.2 software. Percolator was incorporated for peptide validation and ptmRS for PTM localization. Carbamidomethylation (C) was used as fixed modification, and acetylation (K), phosphorylation (STY) and ubiquitination (K) were each used in combination with oxidation (M) as variable modifications in the search parameter fields. Other search parameters included two allowed missed cleavages for trypsin digestion, peptide tolerance at 10 ppm and MS/MS tolerance at 20 mmu. Only peptides with a high identification confidence (PEP < 0.01) and a localization confidence of >99% were taken into account.

Statistics

Results of the Ca^{2+} dependent ATPase measurements were fitted with the Hill function using Origin 8.0. One-way ANOVA with a Bonferroni post-hoc test was used for establishing significance.

Results

Purified SERCA2a from pig heart remains active

We first developed a one-step affinity chromatography protocol to purify native SERCA2a from pig left ventricular tissue, providing a yield of around 2.5 mg per 100 g of heart tissue (Figure 1A). In short, cardiac microsomes were solubilized with DDM, and SERCA2a was purified via Reactive Green affinity chromatography, which captures ATP-binding proteins. SERCA2a was subsequently eluted with AMPPCP. Immunoblotting experiments confirmed that the purified sample consists mainly of the SERCA2a isoform (Figure 1B). Only traces of the housekeeping SERCA2b isoform were found and no SERCA1a was detected (Figure 1B). No bands corresponding to PLB were detected on SDS-PAGE and immunoblotting (Figure 1B). The purified enzyme displayed robust, Ca^{2+}-dependent ATPase activity, with a specific activity of 4.3 ± 0.7 μmoles/min/mg at 1 μM free Ca^{2+}, Hill coefficient n of 1.3 ± 0.1 and K_m value of 0.22 ± 0.01 μM (Figure 1C). Thus, the purified SERCA2a from pig heart remains functional.

E2-AlF_4-CPA and [Ca_2]E1-AMPPCP structures of SERCA2a closely resemble SERCA1a

Structures of cardiac SERCA2a were determined in E2-AlF_4-CPA and [Ca_2]E1-AMPPCP forms at 3.3 Å and 4.0 Å resolution, respectively (Figure 2A, 2B and Table 1). In the [Ca_2]E1-AMPPCP crystals, the TM regions of neighboring proteins interact in an antiparallel packing (*i.e.* not reflecting physiological contacts). However, the E2-AlF_4-CPA crystal form is marked by an unusual parallel packing of SERCA2a molecules involving contact points between the A-domains and N-domains and between the A-domain and the P-domain domains, as well as N-domain and L7/8 (Supplementary Figure 1). No such parallel packing modes have been observed for SERCA1a crystal forms, and many of the involved residues differ for SERCA2a and SERCA1a and are conserved within one isoform. These SERCA2a specific regions may possibly play a role in the dimerization of SERCA2a in cardiomyocytes (Blackwell *et al*, 2016). Note that due to an amino acid deletion in SERCA2a at position 509, the SERCA2a residue numbering from position 509 is shifted by -1 as compared to SERCA1a.

SERCA2a has the same overall domain organization as SERCA1a, including three cytoplasmic domains and 10 TM helices (Figure 2C, 2D). Indeed, the [H_{23}]E2-AlF_4-CPA and [Ca_2]E1-AMPPCP structures of SERCA2a are similar to the corresponding structures of SERCA1a (PDB 3FGO and 3N8G, respectively) (Figure 3A, 3B) with root mean square deviation (r.m.s.d.) for Cα atoms of 0.89 Å and 1.73 Å, respectively. Even the regions of highest sequence diversity, such as luminal loops L7/8 or L9/10 are similarly positioned in SERCA1a and SERCA2a. In both the E1 and E2 structures, the SERCA1a headpiece is tilted more towards the membrane as compared to SERCA2a. The [Ca_2]E1-AMPPCP structure contains clear densities for the AMPPCP molecule as well as for bound Ca^{2+} and K^+

ions. Ca^{2+} and AMPPCP binding in SERCA2a closely resembles the SERCA1a structure (Supplementary Figure 2). The CPA and MgF_x molecules as well as K^+ ions are easily recognized in the E2-AlF_4-CPA structure. However, AMPPCP is not observed despite being present at high concentrations in the crystallization conditions. Similar as in SERCA1a, CPA binds in a groove between helices M2, M3 and M4, coordinated by a Mg^{2+} ion and residues Gln56, Asp59 and Asn101, and blocks the proposed Ca^{2+} entry pathway (Laursen *et al*, 2009).

Isoform specific motifs of SERCA1a and SERCA2a

The catalytic core of the Ca^{2+} pump appears highly conserved (Supplementary Figure 3) indicating that the Ca^{2+} transport mechanism is preserved between SERCA1a and SERCA2a. Despite the 160 amino acid sequence differences between rabbit SERCA1a and pig SERCA2a, their structures do not readily reveal why the isoforms display distinct functional properties. As can be seen from Figures 3C and 3D, the isoform specific sequences are predominantly localized in exposed regions of the N-, P- and A-domains, near the membrane interface of the TM helices M7 and M10, and in the luminal loops L7/8 and L9/10. Based on an alignment of vertebrate SERCA1a and SERCA2a orthologues, many of these sequence differences were found to be highly conserved within one isoform (Supplementary Table 1), indicating that they may exert isoform-specific roles such as to serve as regulatory sites for specific protein or lipid interactions, or post-translational modifications (PTMs).

PLB, the major regulator of SERCA2a, is not present in the structure (Figure 1), but we examined the PLB binding site between M2, M4, M6 and M9 helices in the SERCA2a [H_{2-3}]E2-AlF_4-CPA structure and compared it with the available SERCA1a-PLB and SERCA1a:sarcolipin structures (Akin *et al*, 2013; Winther *et al*, 2013; Toyoshima *et al*, 2013). The SERCA1a complexes adopt Ca^{2+}-free E1 conformations, and the M2 therefore is shifted away by 9.4 Å in SERCA2a, but the relevant sidechains in the PLB binding groove are placed in a similar way (Leu802, Ala806, Phe809, Trp932, Leu939 which interact with Leu31 of PLB; and Gly801, Thr805 and Gln108, which interact with Asn34 of PLB), i.e. not pointing to major differences in the PLB acceptor site in the TM domain of SERCA2a and SERCA1a. We cannot exclude that specific interactions at the N-domain are Other SERCA2a regulators have been described (Vandecaetsbeek *et al*, 2009, 2011; Nelson *et al*, 2016; Anderson *et al*, 2015), but their interaction site are less well characterized.

Isoform specific sites of post-translational modifications

SERCA isoforms are regulated by various PTMs, including sumoylation, phosphorylation, acetylation, glutathionylation, ubiquitination and nitration (Stammers *et al*, 2015). Interestingly, 26 out of the 160

isoform specific residues of SERCA2a (16%) are reported PTM sites supporting the view that many differences in the sequence may serve a regulatory function. Also, a higher number of unique PTMs has been reported for SERCA2a than SERCA1a (87 *versus* 29 reported PTMs). Mapping the previously reported PTMs onto SERCA2a and SERCA1a structures shows that the majority (79/87 in SERCA2a and 27/29 in SERCA1a) of PTMs are located in the cytoplasmic domains, accessible for enzyme interactions (Figure 4A, 4B) (Hornbeck *et al*, 2015).

We experimentally determined which PTMs are present in our purified SERCA1a and SERCA2a samples. With an average coverage of 58.6% for SERCA1a and 60.3% for SERCA2a, MS analysis identified several new PTMs that have not been reported previously. Among these are multiple SERCA2a acetylation sites (Lys128, 205, 234, 352, 371, 451, 492, 628, 712, 727, 757) (Figure 4C, Table 2). In SERCA1a, we found two acetylated residues (Lys205 and 713) and one ubiquitination site (either Lys204 or 205) (Figure 4D, Table 2). However, despite the reported abundance of putative sites for post-translational control in SERCA2a, no additional electron densities were observed in the structures that may be ascribed to PTMs. The absence of PTMs in the electron density maps may be attributed to only low occupancy in the crystal, a high level of disorder, and/or a limited resolution of the structures, as also discussed for the palmitoylation of SERCA1a-SLN (Montigny *et al*, 2014). Additionally, unmodified SERCA2a may have been preferentially incorporated into the crystals during the crystallization process.

Isoform specific sequence differences alter molecular dynamics and functional properties

SERCA2a displays an intrinsically higher Ca^{2+} affinity and lower maximal turnover than SERCA1a (Dode *et al*, 2002, 2003), which should also be attributable to differences in the primary structure. To examine the functional role of the isoform specific sequence differences, we focused on the luminal loop between M7 and M8 helices (L7/8), which shows 15 substitutions on a total of 35 residues. It was shown before that a replacement of L7/8 in SERCA1a by the corresponding loop of SERCA2a (SERCA1a-L7/8) alters the kinetic properties of the protein (Clausen *et al*, 2012). Here, we introduced the SERCA1a-specific L7/8 in SERCA2a (SERCA2a-L7/8-1a chimera) and the SERCA2a-specific L7/8 in SERCA1a (SERCA1a-L7/8-2a chimera) and compared the functional properties of these chimeras with SERCA1a and SERCA2a WT in a COS overexpression system. Expression levels for all constructs were similar (Supplementary Figure 4). We did not observe significant changes in the K_m values of the chimera *versus* their corresponding WT protein, but the substitutions of L7/8 in each isoform significantly reduces the V_{max} by 20-30% (Table 2). While the L7/8 sequence differences alone do not explain the higher V_{max} and K_m of SERCA1a as compared to SERCA2a, the results show that the sequence of L7/8 seems to be only optimal in its own protein core. This suggests that the distinct functional

properties of SERCA2a and SERCA1a relate to a complex interplay between sequence differences at various positions of the protein.

In the absence of clear structural differences between SERCA2a and SERCA1a, we considered that the distinct functional properties of both isoforms may rather relate to different dynamics. To explore this possibility, we compared 50 ns MD simulations of SERCA2a [$H_{2\text{-}3}$]E2-AlF_4^--CPA and its corresponding SERCA1a structure inserted in phosphatidylcholine membranes. The results suggest that isoform specific residues alter intramolecular salt bridge and hydrogen bond interactions that affect the protein dynamics (Supplementary Table 3). Indeed, a significant percentage of salt bridges or hydrogen bonds that are unique to each isoform encompass isoform specific residues: 42.9% in SERCA1a and 28.1% in SERCA2a for salt bridges, and 28.9% of SERCA1a and 39.5% of SERCA2a for hydrogen bonds. Hence, isoform specific residues are overrepresented in distinct networks. With respect to L7/8, we found that residues Val283, His284, and Gly285 of L3/4 in SERCA2a dynamically interact with Lys876 and Asn879 of L7/8 (Figure 5A). These interactions differ from SERCA1a, where Arg290 (L3/4) interacts with Thr877 and Glu878 (L7/8), and Ser287 (L3/4) interacts with the Gln875 and Glu878 (L7/8). Furthermore, residues Glu83 (L1/2), Glu892 (L7/8) and Glu895 (L7/8) of SERCA1a interact with SERCA1a-specific residues of L9/10 (Lys958, Lys958 and Lys960, respectively) (Figure 5B). In both isoforms, Gln965 (Gln966 in SERCA1a) of L9/10 is involved in hydrogen bond interactions with isoform specific residues of L7/8 (Glu895 and Asp861 in SERCA1a and Tyr894 and Gly860 in SERCA2a)with different interaction times (72% and 26%, respectively). (Figure 5A, 5B). Thus, the isoform specific dynamic behavior of L7/8 depends on interactions with neighboring loops L3/4 and L9/10, which may explain why replacing L7/8 in both the SERCA1a-L7/8-2a and SERCA2a-L7/8-1a chimeras is associated with a loss of function.

Discussion

In this study, we developed a high yield purification protocol of native SERCA2a from pig heart and determined the first crystal structures representing two conformational state. We combined structural information, MD simulations, mass spectrometry, and a biochemical analysis to compare it to the muscle specific Ca^{2+}-ATPases, SERCA1a.

Role of SERCA2a and SERCA1a specific sequences

The good resemblance between SERCA2a and SERCA1a structures is consistent with a highly conserved Ca^{2+} transport mechanism in the two isoforms. However, we show that the sequence variations in SERCA2a and SERCA1a are functionally relevant, alter the dynamics, and allow isoform specific

regulatory control. The conserved structure indicates that it may be possible to study the functional role of the isoform sequences by generating chimera proteins of SERCA1a and SERCA2a. However, we notice that the functional effect of isoform specific regions depends on the structural context, which is also isoform specific. We further depict that many sites for PTMs are located in exposed regions of the pumps and are isoform specific, indicating that these unique sequences support regulatory control. It is well established that SERCA2a is regulated by an increasing number of PTMs, and that this regulatory control may be disturbed in pathological conditions such as HF (Kho *et al*, 2011). For instance, the progressive accumulation of SERCA2a tyrosine nitration has been described during aging (Viner *et al*, 1999) and SERCA2a nitration levels are clearly correlated with HF (Lokuta *et al*, 2005). Moreover, nitration of SERCA2a-containing microsomes has a strong negative effect on Ca^{2+} uptake (Lokuta *et al*, 2005), and sumoylation regulates SERCA2a activity and stability and is decreased in HF, while restoration of SERCA2a sumoylation provides cardioprotection (Kho *et al*, 2011). An increased SERCA2a acetylation is associated with higher activity and altered intracellular Ca^{2+} dynamics influencing performance of cardiomyocytes (Meraviglia *et al*, 2018). The growing number of PTMs represents a major challenge to decipher the functional impact of each individual modification. A future assessment of the SERCA2a PTM profile of SERCA2a isolated from healthy and diseased hearts will allow us to establish a fingerprint of different SERCA2a PTMs in disease and pinpoint their effect on local and global dynamics of SERCA2a.

One of the most varying regions between SERCA1a and SERCA2a at the luminal side of the membrane is L7/8, which appears to be an important regulatory site. SERCA isoforms are regulated by a disulfide bridge formed between two conserved Cys residues on L7/8 (Daiho *et al*, 2001; Ushioda *et al*, 2016). In SERCA1a, the disulfide bridge inactivates the pump activity, while in SERCA2b, the reversible formation of a disulfide bridge between C875 and C887 serves as a luminal redox sensor that is controlled by an ER disulfide reductase (Ushioda *et al*, 2016). Furthermore, binding of calumenin to L7/8 leads to a reduction in the apparent Ca^{2+} affinity of the ATPase (Sahoo *et al*, 2009). In addition, only in SERCA2 isoforms L7/8 serves as an acceptor site for the luminal extension of the SERCA2b C-terminus, indicating that L7/8 is important for the isoform specific properties. The functional analysis of this study shows that a simple replacement of L7/8 reduces the maximal turnover rate in both the SERCA1a and SERCA2a backgrounds. According to previous kinetic measurements, L7/8 of SERCA2a lowers the Ca^{2+} dissociation rate towards the cytosol, and the rate of the E2 to E1 conversion is also reduced (Clausen *et al*, 2012). Together this suggests that L7/8 is adapted to the local environment in each isoform, which is confirmed by the MD simulations that highlight dynamic interactions between L3/4 and the isoform specific loops L7/8 and L9/10.

Mapping Darier disease mutations on the SERCA2a structure

Several mutations in the *ATP2A2* gene are associated with Darier's disease (DD), an autosomal dominant skin disorder, which is characterized by keratosis, skin and nail defects (Sakuntabhai *et al*, 1999b). Here, we used the SERCA2a structures to map all known DD mutations of various disease impact (Stenson *et al*, 2017). The map demonstrates that DD mutations are scattered all over the protein, without specific clusters that correlate with disease severity (Figure 6). DD mutations affect SERCA2a/b activity by a reduced protein stability and/or impaired functionality, which point to haploinsufficiency explaining the dominant inheritance pattern. Although DD mutations affect all three SERCA2 splice variants (SERCA2a-c), clinical manifestations only appear in the skin, where the ubiquitous SERCA2b isoform is expressed, while cardiac functionality is surprisingly well preserved (Tavadia *et al*, 2001; Mayosi *et al*, 2006).

Conclusion

The first structures of the SERCA2a isoform presented here represent important steps to facilitate further structural and functional studies of SERCA2a in normal and diseased context. SERCA2a is a favorable and recognized target for HF therapy, and the study also opens the door for the future crystallization of SERCA2a complexes with small molecules or TM regulators like PLB, which will aid drug discovery efforts. The SERCA2a and SERCA1a structures are very similar, which indicates a conserved mechanism of Ca^{2+} transport, but the isoform specific sequence differences introduce unique sites of regulation and may alter the molecular dynamics and kinetic behavior of the pump in different tissues. These insights may be of interest for drug discovery efforts to develop SERCA2a specific modulators, which will also be facilitated by the availability of the SERCA2a structural information.

Acknowledgements

We would like to thank Maike Bublitz and Jesper Lykkegaard Karlsen for their help with data processing and iMDff experiments. We are grateful to Marleen Schuermans, Ingrid Puusta, Boyin Liu, Tugce Arslan, Anne Lindeman, Anna Marie Nielsen, Lotte Thue Pedersen and Tetyana Klymchuk for their excellent technical assistance. Also, we would like to thank Howard Young for the initial input to establish a purification protocol. We would like to thank the Swiss Light Source (Paul Scherrer Institute) for providing data-collection facilities, and the EMBL beamlines at ESRF and DESY for crystal screening. This work was funded by the Flanders Research Foundation FWO (G044212N and G0B1115N), and the Inter-University Attraction Poles program (P7/13) assigned to PV. The work was supported by an ERC grant (BIOMEMOS) to PN. The DANDRITE center is funded by the Lundbeck

Foundation (grant no. R248-2016-2518). AS was supported by the IWT doctoral scholarship provided by Agentschap Innoveren & Ondernemen (VLAIO).

References

Adams PD, Afonine P V, Bunkóczi G, Chen VB, Davis IW, Echols N, Headd JJ, Hung L-W, Kapral GJ, Grosse-Kunstleve RW, McCoy AJ, Moriarty NW, Oeffner R, Read RJ, Richardson DC, Richardson JS, Terwilliger TC & Zwart PH (2010) PHENIX: a comprehensive Python-based system for macromolecular structure solution. *Acta Crystallogr. D. Biol. Crystallogr.* **66:** 213–21

Akin BL, Hurley TD, Chen Z & Jones LR (2013) The structural basis for phospholamban inhibition of the calcium pump in sarcoplasmic reticulum. *J. Biol. Chem.* **288:** 30181–30191

Albers RW, Fahn S & Koval GJ (1963) The role of sodium ions in the activation of electrophorus electric organ adenosine triphosphatase. *Proc. Natl. Acad. Sci. U. S. A.* **50:** 474–81

Anderson DM, Anderson KM, Chang CL, Makarewich CA, Nelson BR, McAnally JR, Kasaragod P, Shelton JM, Liou J, Bassel-Duby R & Olson EN (2015) A micropeptide encoded by a putative long noncoding RNA regulates muscle performance. *Cell* **160:** 595–606

Anderson DM, Makarewich CA, Anderson KM, Shelton JM, Bezprozvannaya S, Bassel-Duby R & Olson EN (2016) Widespread control of calcium signaling by a family of SERCA-inhibiting micropeptides. *Sci. Signal.* **9:**

Arkin IT, Adams PD, MacKenzie KR, Lemmon MA, Brünger AT & Engelman DM (1994) Structural organization of the pentameric transmembrane alpha-helices of phospholamban, a cardiac ion channel. *EMBO J.* **13:** 4757–4764

Axelsen KB & Palmgren MG (1998) Evolution of substrate specificities in the P-type ATPase superfamily. *J. Mol. Evol.* **46:** 84–101

Baginski ES, Foà PP & Zak B (1967) Microdetermination of inorganic phosphate, phospholipids, and total phosphate in biologic materials. *Clin. Chem.* **13:** 326–32

Bers DM (2002) Cardiac excitation contraction coupling. *Nature* **415:** 198–215

Blackwell DJ, Zak TJ & Robia SL (2016) Cardiac Calcium ATPase Dimerization Measured by Cross-Linking and Fluorescence Energy Transfer. *Biophys. J.* **111:** 1192–1202

Bublitz M, Musgaard M, Poulsen H, Thøgersen L, Olesen C, Schiøtt B, Morth JP, Møller JV & Nissen P (2013) Ion pathways in the sarcoplasmic reticulum Ca2+-ATPase. *J. Biol. Chem.* **288:** 10759–65

Bublitz M, Poulsen H, Morth JP & Nissen P (2010) In and out of the cation pumps: P-type ATPase structure revisited. *Curr. Opin. Struct. Biol.* **20:** 431–9

Chao SC, Yang MH & Lee JYY (2002) Mutation analysis of the ATP2A2 gene in Taiwanese patients with Darier's disease. *Br. J. Dermatol.* **146:** 958–963

Clausen JD, Vandecaetsbeek I, Wuytack F, Vangheluwe P & Andersen JP (2012) Distinct roles of the C-terminal 11th transmembrane helix and luminal extension in the partial reactions determining the high Ca2+ affinity of sarco(endo)plasmic reticulum Ca2+-ATPase isoform 2b (SERCA2b). *J. Biol. Chem.* **287:** 39460–39469

Croll TI & Andersen GR (2016) Re-evaluation of low-resolution crystal structures via interactive molecular-dynamics flexible fitting (iMDFF): a case study in complement C4. *Acta Crystallogr. Sect. D Struct. Biol.* **72:** 1006–1016

Daiho T, Yamasaki K, Saino T, Kamidochi M, Satoh K, Iizuka H & Suzuki H (2001) Mutations of either or both Cys876 and Cys888 residues of sarcoplasmic reticulum Ca2+-ATPase result in a complete loss of Ca2+ transport activity without a loss of Ca2+-dependent ATPase activity. Role of the CYS876-CYS888 disulfide bond. *J. Biol. Chem.* **276:** 32771–8

Dode L, Andersen JP, Leslie N, Dhitavat J, Vilsen B & Hovnanian A (2003) Dissection of the functional differences between sarco(endo)plasmic reticulum Ca2+-ATPase (SERCA) 1 and 2 isoforms and characterization of Darier disease (SERCA2) mutants by steady-state and transient kinetic analyses. *J. Biol. Chem.* **278:** 47877–89

Dode L, Vilsen B, Van Baelen K, Wuytack F, Clausen JD & Andersen JP (2002) Dissection of the functional differences between sarco(endo)plasmic reticulum Ca2+-ATPase (SERCA) 1 and 3

isoforms by steady-state and transient kinetic analyses. *J. Biol. Chem.* **277:** 45579–91

Emsley P & Cowtan K (2004) Coot: model-building tools for molecular graphics. *Acta Crystallogr. Sect. D Biol. Crystallogr.* **60:** 2126–2132

Ferrandi M, Barassi P, Tadini-Buoninsegni F, Bartolommei G, Molinari I, Tripodi MG, Reina C, Moncelli MR, Bianchi G & Ferrari P (2013) Istaroxime stimulates SERCA2a and accelerates calcium cycling in heart failure by relieving phospholamban inhibition. *Br. J. Pharmacol.* **169:** 1849–61

Focht D, Croll TI, Pedersen BP & Nissen P (2017) Improved Model of Proton Pump Crystal Structure Obtained by Interactive Molecular Dynamics Flexible Fitting Expands the Mechanistic Model for Proton Translocation in P-Type ATPases. *Front. Physiol.* **8:** 202

Foster DB, Liu T, Rucker J, O'Meally RN, Devine LR, Cole RN & O'Rourke B (2013) The Cardiac Acetyl-Lysine Proteome. *PLoS One* **8:** e67513

Greenberg B, Butler J, Felker GM, Ponikowski P, Voors AA, Desai AS, Barnard D, Bouchard A, Jaski B, Lyon AR, Pogoda JM, Rudy JJ & Zsebo KM (2016) Calcium upregulation by percutaneous administration of gene therapy in patients with cardiac disease (CUPID 2): A randomised, multinational, double-blind, placebo-controlled, phase 2b trial. *Lancet* **387:** 1178–1186

Haghighi K, Kolokathis F, Pater L, Lynch RA, Asahi M, Gramolini AO, Fan G-C, Tsiapras D, Hahn HS, Adamopoulos S, Liggett SB, Dorn GW, MacLennan DH, Kremastinos DT & Kranias EG (2003) Human phospholamban null results in lethal dilated cardiomyopathy revealing a critical difference between mouse and human. *J. Clin. Invest.* **111:** 869–76

Hess B, Kutzner C, Van Der Spoel D & Lindahl E (2008) GRGMACS 4: Algorithms for highly efficient, load-balanced, and scalable molecular simulation. *J. Chem. Theory Comput.* **4:** 435–447

Hornbeck P V., Zhang B, Murray B, Kornhauser JM, Latham V & Skrzypek E (2015) PhosphoSitePlus, 2014: mutations, PTMs and recalibrations. *Nucleic Acids Res.* **43:** D512–D520

Hulot JS, Salem JE, Redheuil A, Collet JP, Varnous S, Jourdain P, Logeart D, Gandjbakhch E, Bernard C, Hatem SN, Isnard R, Cluzel P, Le Feuvre C, Leprince P, Hammoudi N, Lemoine FM, Klatzmann D, Vicaut E, Komajda M, Montalescot G, et al (2017) Effect of intracoronary administration of AAV1/SERCA2a on ventricular remodelling in patients with advanced systolic heart failure: Results from the AGENT-HF randomized phase 2 trial. *Eur. J. Heart Fail.*

Jessup M, Greenberg B, Mancini D, Cappola T, Pauly DF, Jaski B, Yaroshinsky A, Zsebo KM, Dittrich H, Hajjar RJ & Calcium Upregulation by Percutaneous Administration of Gene Therapy in Cardiac Disease (CUPID) Investigators (2011) Calcium Upregulation by Percutaneous Administration of Gene Therapy in Cardiac Disease (CUPID): a phase 2 trial of intracoronary gene therapy of sarcoplasmic reticulum Ca2+-ATPase in patients with advanced heart failure. *Circulation* **124:** 304–13

Jorgensen WL, Chandrasekhar J, Madura JD, Impey RW & Klein ML (1983) Comparison of simple potential functions for simulating liquid water. *J. Chem. Phys.* **79:** 926–935

Kabsch W (2010) XDS. *Acta Crystallogr. D. Biol. Crystallogr.* **66:** 125–32

Kaneko M, Yamamoto H, Sakai H, Kamada Y, Tanaka T, Fujiwara S, Yamamoto S, Takahagi H, Igawa H, Kasai S, Noda M, Inui M & Nishimoto T (2017) A pyridone derivative activates SERCA2a by attenuating the inhibitory effect of phospholamban. *Eur. J. Pharmacol.*

Kho C, Lee A, Jeong D, Oh JG, Chaanine AH, Kizana E, Park WJ & Hajjar RJ (2011) SUMO1-dependent modulation of SERCA2a in heart failure. *Nature* **477:** 601–605

Kim W, Bennett EJ, Huttlin EL, Guo A, Li J, Possemato A, Sowa ME, Rad R, Rush J, Comb MJ, Harper JW & Gygi SP (2011) Systematic and quantitative assessment of the ubiquitin-modified proteome. *Mol. Cell* **44:** 325–340

Kimura Y, Asahi M, Kurzydlowski K, Tada M & MacLennan DH (1998) Phospholamban Domain Ib Mutations Influence Functional Interactions with the Ca2+-ATPase Isoform of Cardiac Sarcoplasmic Reticulum. *J. Biol. Chem.* **273:** 14238–14241

Laursen M, Bublitz M, Moncoq K, Olesen C, Møller JV, Young HS, Nissen P & Morth JP (2009) Cyclopiazonic acid is complexed to a divalent metal ion when bound to the sarcoplasmic reticulum Ca2+-ATPase. *J. Biol. Chem.* **284:** 13513–8

Lokuta AJ, Maertz NA, Meethal SV, Potter KT, Kamp TJ, Valdivia HH & Haworth RA (2005) Increased nitration of sarcoplasmic reticulum Ca2+-ATPase in human heart failure. *Circulation*

111: 988–995

Lundby A, Lage K, Weinert BT, Bekker-Jensen DB, Secher A, Skovgaard T, Kelstrup CD, Dmytriyev A, Choudhary C, Lundby C & Olsen J V. (2012a) Proteomic Analysis of Lysine Acetylation Sites in Rat Tissues Reveals Organ Specificity and Subcellular Patterns. *Cell Rep*. **2:** 419–431

Lundby A, Secher A, Lage K, Nordsborg NB, Dmytriyev A, Lundby C & Olsen J V. (2012b) Quantitative maps of protein phosphorylation sites across 14 different rat organs and tissues. *Nat. Commun*. **3:**

MacLennan DH & Kranias EG (2003) Phospholamban: a crucial regulator of cardiac contractility. *Nat. Rev. Mol. Cell Biol*. **4:** 566–577

Maruyama K & MacLennan DH (1988) Mutation of aspartic acid-351, lysine-352, and lysine-515 alters the Ca2+ transport activity of the Ca2+-ATPase expressed in COS-1 cells. *Proc. Natl. Acad. Sci. U. S. A*. **85:** 3314–8

Mayosi BM, Kardos A, Davies CH, Gumedze F, Hovnanian A, Burge S, Watkins H & Watkins H (2006) Heterozygous disruption of SERCA2a is not associated with impairment of cardiac performance in humans: implications for SERCA2a as a therapeutic target in heart failure. *Heart* **92:** 105–109

McCoy AJ, Grosse-Kunstleve RW, Adams PD, Winn MD, Storoni LC & Read RJ (2007) *Phaser* crystallographic software. *J. Appl. Crystallogr*. **40:** 658–674

Meraviglia V, Bocchi L, Sacchetto R, Florio M, Motta B, Corti C, Weichenberger C, Savi M, D'Elia Y, Rosato-Siri M, Suffredini S, Piubelli C, Pompilio G, Pramstaller P, Domingues F, Stilli D & Rossini A (2018) HDAC Inhibition Improves the Sarcoendoplasmic Reticulum Ca2+-ATPase Activity in Cardiac Myocytes. *Int. J. Mol. Sci*. **19:** 419

Mertins P, Qiao JW, Patel J, Udeshi ND, Clauser KR, Mani DR, Burgess MW, Gillette MA, Jaffe JD & Carr SA (2013) Integrated proteomic analysis of post-translational modifications by serial enrichment. *Nat. Methods* **10:** 634–637

Miyauchi Y, Daiho T, Yamasaki K, Takahashi H, Ishida-Yamamoto A, Danko S, Suzuki H & Iizuka H (2006) Comprehensive analysis of expression and function of 51 sarco(endo)plasmic reticulum Ca2+-ATPase mutants associated with darier disease. *J. Biol. Chem*. **281:** 22882–22895

Moller J V., Olesen C, Winther A-ML & Nissen P (2010) The sarcoplasmic Ca(2+)-ATPase: design of a perfect chemi-osmotic pump. *Q. Rev. Biophys*. **43:** 501–566

Montigny C, Decottignies P, Le Maréchal P, Capy P, Bublitz M, Olesen C, Møller JV, Nissen P & Le Maire M (2014) S-Palmitoylation and S-Oleoylation of Rabbit and Pig Sarcolipin *. *Publ. JBC Pap. Press*

Mountian I, Baba-aı F, Jonas J, Smedt H De, Wuytack F & Parys JB (2001) Expression of Ca 2 ⁒ Transport Genes in Platelets and Endothelial Cells in Hypertension. **:** 135–141

Nellen RGL, Steijlen PM, van Steensel MAM, Vreeburg M, Frank J, van Geel M & van Geel M (2017) Mendelian Disorders of Cornification Caused by Defects in Intracellular Calcium Pumps: Mutation Update and Database for Variants in ATP2A2 and ATP2C1 Associated with Darier Disease and Hailey-Hailey Disease. *Hum. Mutat*. **38:** 343–356

Nelson BR, Makarewich CA, Anderson DM, Winders BR, Troupes CD, Wu F, Reese AL, McAnally JR, Chen X, Kavalali ET, Cannon SC, Houser SR, Bassel-Duby R & Olson EN (2016) A peptide encoded by a transcript annotated as long noncoding RNA enhances SERCA activity in muscle. *Sci. AAAS* **351:** 271–275

Periasamy M, Bhupathy P & Babu GJ (2008) Regulation of sarcoplasmic reticulum Ca2+ ATPase pump expression and its relevance to cardiac muscle physiology and pathology. *Cardiovasc. Res*. **77:** 265–73

Post RL & Sen AK (1965) An Enzymatic Mechanism of Active Sodium and Potassium Transport. *J. Histochem. Cytochem*. **13:** 105–12

Ren YQ, Gao M, Liang YH, Hou YX, Wang PG, Sun LD, Xu SX, Li W, Du WH, Zhou FS, Shen YJ, Yang S & Zhang XJ (2006) Five mutations of ATP2A2 gene in Chinese patients with Darier's disease and a literature review of 86 cases reported in China. *Arch. Dermatol. Res*. **298:** 58–63

Ringpfeil F, Raus a, DiGiovanna JJ, Korge B, Harth W, Mazzanti C, Uitto J, Bale SJ & Richard G (2001) Darier disease--novel mutations in ATP2A2 and genotype-phenotype correlation. *Exp. Dermatol*. **10:** 19–27

Ruiz-Perez VL, Carter SA, Healy E, Todd C, Rees JL, Steijlen PM, Carmichael AJ, Lewis HM, Hohl

D, Itin P, Vahlquist A, Gobello T, Mazzanti C, Reggazini R, Nagy G, Munro CS & Strachan T (1999) ATP2A2 mutations in Darier's disease: Variant cutaneous phenotypes are associated with missense mutations, but neuropsychiatric features are independent of mutation class. *Hum. Mol. Genet.* **8:** 1621–1630

Sahoo SK, Kim T, Kang GB, Lee JG, Eom SH & Kim DH (2009) Characterization of calumenin-SERCA2 interaction in mouse cardiac sarcoplasmic reticulum. *J. Biol. Chem.* **284:** 31109–31121

Sakuntabhai A, Burge S, Monk S & Hovnanian A (1999a) Spectrum of novel ATP2A2 mutations in patients with Darier's disease. *Hum. Mol. Genet.* **8:** 1611–1619

Sakuntabhai A, Ruiz-Perez V, Carter S, Jacobsen N, Burge S, Monk S, Smith M, Munro CS, O 'donovan M, Craddock N, Kucherlapati R, Rees JL, Owen M, Lathrop GM, Monaco AP, Strachan T & Hovnanian A (1999b) Mutations in ATP2A2, encoding a Ca 2+ pump, cause Darier disease. *Nat. Genet.* **21:** 271–277

Sorensen TL & Andersen JP (2000) Importance of stalk segment S5 for intramolecular communication in the sarcoplasmic reticulum Ca2+-ATPase. *J. Biol. Chem.* **275:** 28954–61

Stammers AN, Susser SE, Hamm NC, Hlynsky MW, Kimber DE, Kehler DS & Duhamel TA (2015) The regulation of sarco(endo)plasmic reticulum calcium-ATPases (SERCA). *Can. J. Physiol. Pharmacol.* **12:** 1–12

Stenson PD, Mort M, Ball E V, Evans K, Hayden M, Heywood S, Hussain M, Phillips AD & Cooper DN (2017) The Human Gene Mutation Database: towards a comprehensive repository of inherited mutation data for medical research, genetic diagnosis and next-generation sequencing studies. *Hum. Genet.* **136:** 665–677

Tavadia S, Tait RC, McDonagh TA & Munro CS (2001) Platelet and cardiac function in Darier's disease. *Clin. Exp. Dermatol.* **26:** 696–9

Toyoshima C, Iwasawa S, Ogawa H, Hirata A, Tsueda J & Inesi G (2013) Crystal structures of the calcium pump and sarcolipin in the Mg2+-bound E1 state. *Nature* **495:** 260–4

Trieber CA, Douglas JL, Afara M & Young HS (2005) The Effects of Mutation on the Regulatory Properties of Phospholamban in Co-Reconstituted Membranes. *Biochemistry* **44:** 3289–3297

Ushioda R, Miyamoto A, Inoue M, Watanabe S, Okumura M, Maegawa K, Uegaki K, Fujii S, Fukuda Y, Umitsu M, Takagi J, Inaba K, Mikoshiba K & Nagata K (2016) Redox-assisted regulation of Ca^{2+} homeostasis in the endoplasmic reticulum by disulfide reductase ERdj5. *Proc. Natl. Acad. Sci.* **113:** E6055–E6063

Vandecaetsbeek I, Raeymaekers L, Wuytack F & Vangheluwe P (2009) Factors controlling the activity of the SERCA2a pump in the normal and failing heart. *Biofactors* **35:** 484–99

Vandecaetsbeek I, Vangheluwe P, Raeymaekers L, Wuytack F & Vanoevelen J (2011) The Ca2+ pumps of the endoplasmic reticulum and Golgi apparatus. *Cold Spring Harb. Perspect. Biol.* **3:** 1–24

Vangheluwe P, Schuermans M, Zádor E, Waelkens E, Raeymaekers L & Wuytack F (2005) Sarcolipin and phospholamban mRNA and protein expression in cardiac and skeletal muscle of different species. *Biochem. J.* **389:** 151–9

Viner RI, Ferrington DA, Williams TD, Bigelow DJ & Scho C (1999) Protein modification during biological aging : selective tyrosine nitration of the SERCA2a isoform of the sarcoplasmic reticulum Ca 2 +-ATPase in skeletal muscle. *Biochem. J* **340:** 657–669

Wagner SA, Beli P, Weinert BT, Schölz C, Kelstrup CD, Young C, Nielsen ML, Olsen J V., Brakebusch C & Choudhary C (2012) Proteomic Analyses Reveal Divergent Ubiquitylation Site Patterns in Murine Tissues. *Mol. Cell. Proteomics* **11:** 1578–1585

Winther A-ML, Bublitz M, Karlsen JL, Møller J V, Hansen JB, Nissen P & Buch-Pedersen MJ (2013) The sarcolipin-bound calcium pump stabilizes calcium sites exposed to the cytoplasm. *Nature* **495:** 265–9

Wu Q, Cheng Z, Zhu J, Xu W, Peng X, Chen C, Li W, Wang F, Cao L, Yi X, Wu Z, Li J & Fan P (2015) Suberoylanilide hydroxamic acid treatment reveals crosstalks among proteome, ubiquitylome and acetylome in non-small cell lung cancer A549 cell line. *Sci. Rep.* **5:**

Yao Q, Chen LT & Bigelow DJ (1998) Affinity purification of the Ca-ATPase from cardiac sarcoplasmic reticulum membranes. *Protein Expr. Purif.* **13:** 191–7

Young HS, Rigaud JL, Lacapère JJ, Reddy LG & Stokes DL (1997) How to make tubular crystals by reconstitution of detergent-solubilized Ca2+-ATPase. *Biophys. J.* **72:** 2545–2558

Zhao X, León IR, Bak S, Mogensen M, Wrzesinski K, Højlund K & Jensen ON (2011) Phosphoproteome Analysis of Functional Mitochondria Isolated from Resting Human Muscle Reveals Extensive Phosphorylation of Inner Membrane Protein Complexes and Enzymes. *Mol. Cell. Proteomics* **10:** M110.000299

Figures

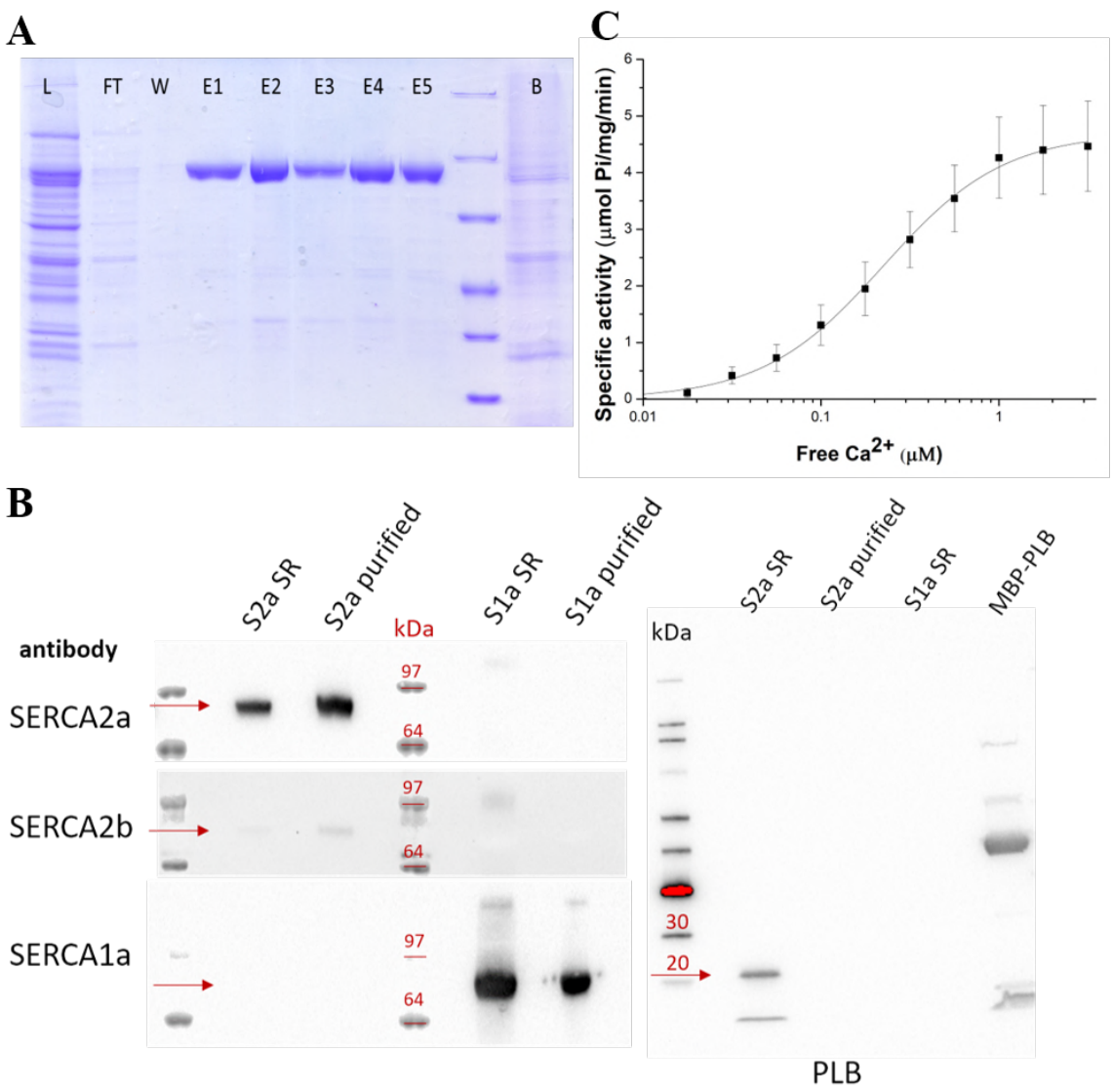

Figure 1. SERCA2a purification and activity

A. SDS-PAGE of fractions of the SERCA2a purification procedure (Load, total lysate; FT, flow-through from Reactive Green beads; Elution, elution fractions; Beads, beads after elution). B. Immunoblot with Sarcoplasmic Reticulum (SR) preparations of cardiac (S2a SR) and skeletal muscle (S1a SR), and purified SERCA2a (S2a purified) and SERCA1a (S1a purified). Detection was performed using antibodies against three SERCA isoforms 1a, 2a and 2b; or phospholamban (PLB). PLB appears as a monomeric (5 kDa) and pentameric band (25 kDa). A fusion construct of PLB with maltose binding protein (MBP) was used as a positive control for PLB detection. C. Ca^{2+}-dependent ATPase activity of the purified SERCA2a. K_m=0.22 ± 0.01 μM, specific activity is 4.3 ± 0.7 μmoles/min/mg at 1 μM free Ca^{2+}, Hill coefficient n of 1.3.

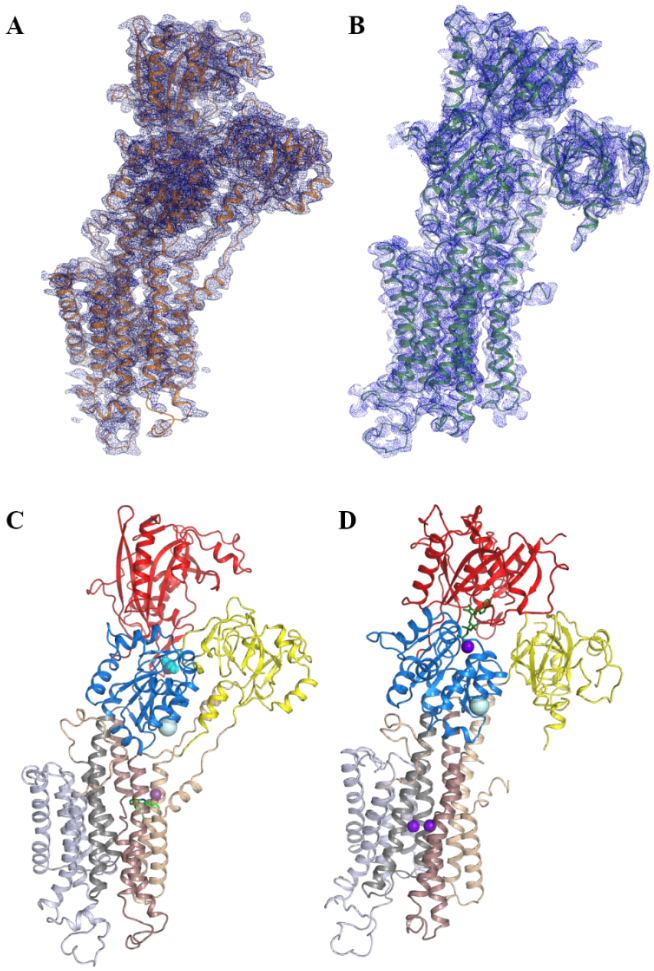

Figure 2. Crystal structures of cardiac SERCA2a in the E2-AlF_4^--CPA and [Ca_2]E1-AMPPCP conformational states

Electron density maps of the SERCA2a E2-AlF_4^-CPA (A) and [Ca_2]E1-AMPPCP (B) structures. Domain-colored SERCA2a in E2-AlF_4^-CPA (C) and [Ca_2]E1-AMPPCP (D) states: A domain is colored in yellow, P in blue and N in red. M1-M2 are colored in wheat, M3-M4 in brown, M5-M6 in dark grey, and M7-M10 in light grey. Ca^{2+}/Mg^{2+} ions are represented in purple spheres, AMPPCP in green sticks. The E2-AlF_4^--CPA structure depicts 992 amino acids of the 997 (no electron density was observed for the last five amino acids). The model of SERCA2a in the E1-Ca^{2+}-AMPPCP conformational state contains 993 amino acids (Glu2-Gly994) of 997 total, with the exception of the residues Leu41-Leu49, Arg134-Lys135, Met239-Gln244, Ala424-Leu425, Ser504-Ser509, which were not build due to lack of electron density features.

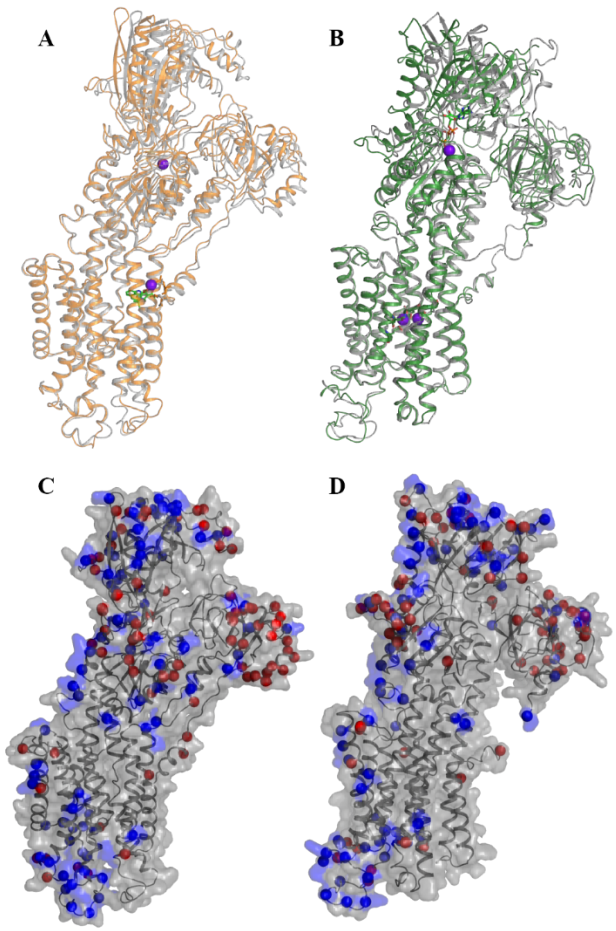

Figure 3. Comparison of the SERCA2a structures with the SERCA1a structures in the corresponding conformational states (PDB 3FGO and 3N8G)

A. Alignment of the SERCA2a E2-AlF_4^--CPA (orange) and SERCA1a (grey) structures. B. Alignment of the SERCA2a [Ca_2]E1-AMPPCP (green) and SERCA1a (grey) structures C, D. Isoform specific residues are represented by both red and blue spheres mapped on the SERCA2a E2-AlF_4^--CPA (C) and [Ca_2]E1-AMPPCP (D) structures. Blue spheres depict residues that are identical in more than 90% of a selection of 83 vertebrate orthologues, while red spheres are less conserved.

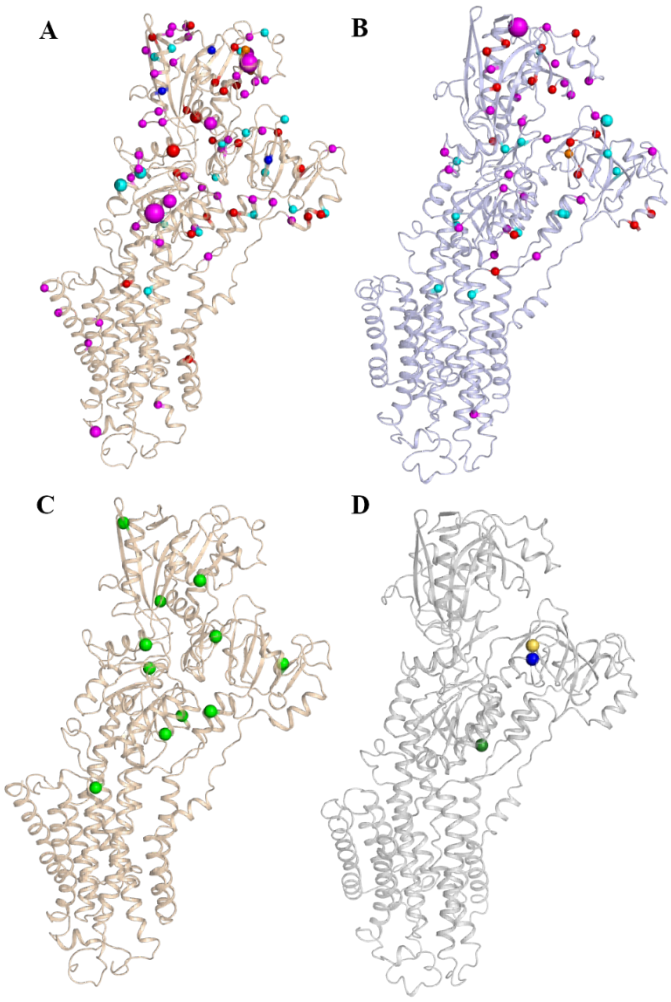

Figure 4. Post-translational modifications mapped on SERCA2a and SERCA1a structures

Post-translational modifications (PTMs) that were reported previously in human, mouse and rat (Hornbeck *et al*, 2015; Foster *et al*, 2013), as well as found in this study (in rabbit and pig) are shown in spheres for SERCA2a E2-AlF_4-CPA (A) and SERCA1a (PDB 3FGO) (B). Phosphorylation is shown in magenta spheres, ubiquitination in cyan, sumoylation in orange, acetylation in red and methylation in dark blue spheres. The size of the sphere correlates with the number of records obtained via a proteomic discovery-mode mass spectrometry approach (the smallest sized spheres correspond to PTMs that were identified one to five times, the medium sized sphere represents 6-25 hits and the largest sized spheres indicate >26 records). C. Newly identified acetylation sites found in purified SERCA2a in this study are shown in green spheres. D. Newly identified PTMs in purified SERCA1a by MS in this study: Lys204 (blue sphere) or Lys205 (yellow sphere) was found ubiquitinated, as well as Lys205 and Lys713 (green sphere) were found acetylated.

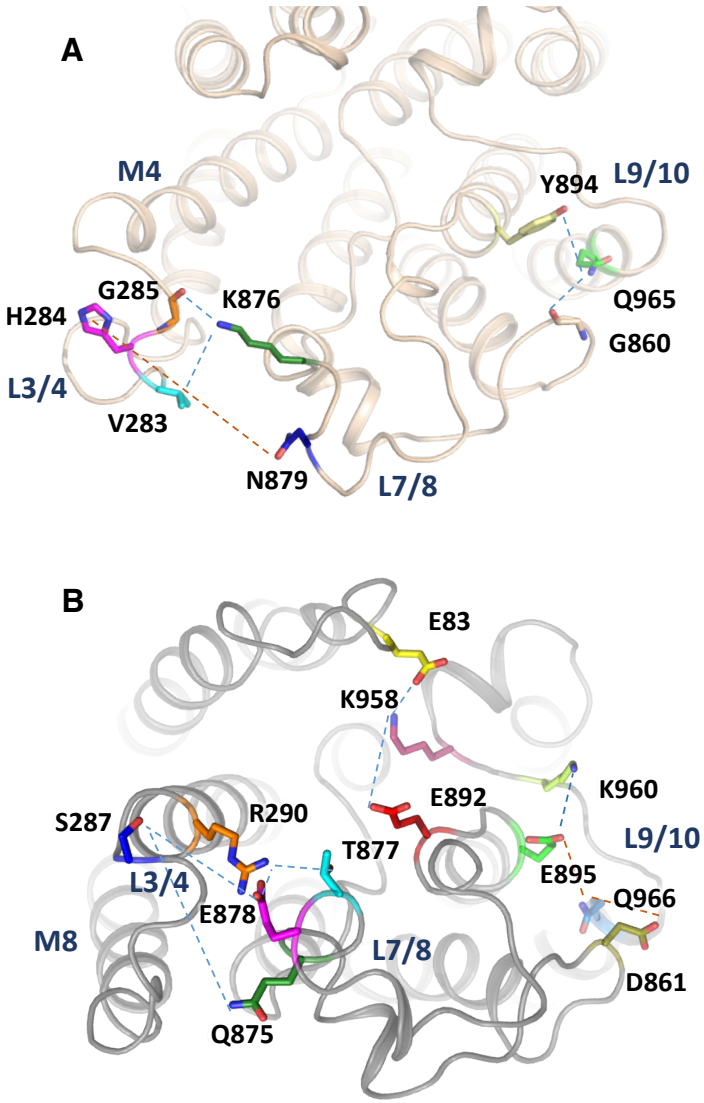

Figure 5. Residues of the luminal loops involved in isoform specific interactions according to molecular dynamics simulation

A. SERCA2a in the E2-AlF_4-CPA state depicting SERCA2a-specific residues involved in isoform unique interactions during MD simulations. B. SERCA1a (PDB 3FGO) depicting SERCA1a-specific residues involved in isoform unique interactions during MD simulations. The two panels are shown from the luminal side on the membrane, but in slightly different orientations for clarity on involved residues.

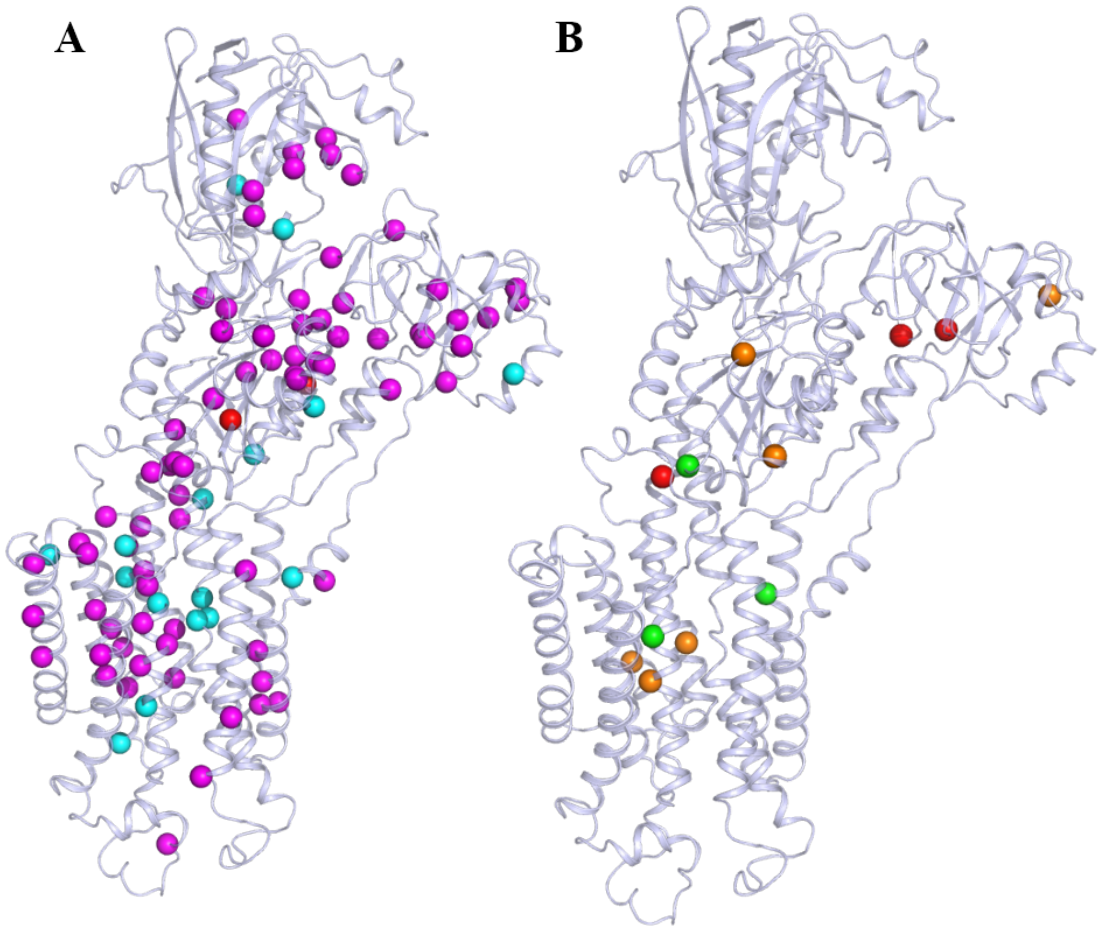

Figure 6. Darier-disease mutations

A. Darier disease (DD)-associated mutations shown in magenta spheres are missense/nonsense mutations, in cyan are most likely DD mutations and in red are associated with acrokeratosis verruciformis/hypertension. B. The review of Nellen *et al*. correlates DD mutations with the severity of the phenotype (Nellen *et al*, 2017). Mutations leading to a mild phenotype are represented by green spheres, moderate by orange and severe by red. Some of the mutations with the described severe (Pro160, Gly211, Gln691, Arg750, His943) and moderate phenotypes (His943, Asn795, Gly769, Gln691, Ala672, Arg131) are associated with lower expression and activity levels of the protein (e.g. Arg750, His943 and Arg131) (Sorensen & Andersen, 2000; Ruiz-Perez *et al*, 1999; Miyauchi *et al*, 2006; Sakuntabhai *et al*, 1999a; Ringpfeil *et al*, 2001; Chao *et al*, 2002). Also, Gly211 is related with the slower turnover rate of the protein and Gly769 with a higher affinity and Ca^{2+} transport (Ruiz-Perez *et al*, 1999; Miyauchi *et al*, 2006; Ren *et al*, 2006).

Table 1. Data collection and refinement statistics for the SERCA2a structures in the Ca^{2+}-E1-AMPPCP and E2-AlF_4^--CPA conformational states.

	[Ca_2]E1-AMPPCP	**[H_{2-3}]E2-AlF_4^--CPA**
Data collection		
Resolution range (Å)	42.7 – 4.0 (4.5 – 4.0)	63.3 – 3.3 (3.35 – 3.3)
Space group	P 2	P 2_1
Cell dimensions		
a, b, c (Å)	117.0, 51.8, 125.6	53.35 253.3 65.0
α, β, γ (°)	90, 106.1, 90	90.0 100.9 90.0
Mosaicity (^{0})	0.38	0.17
Total reflections	45415 (12237)	86319 (16193)
Unique reflections	12416 (3443)	25135 (4544)
Multiplicity	3.7 (3.6)	3.4 (3.6)
Completeness (%)	98.7 (98.3)	99.0 (99.0)
Mean I/σ(I)	4.2 (0.9)	7.1 (1.0)
Molecules per ASU	1	1
R_{merge}	0.293 (>1)	0.130 (>1)
R_{pim}	0.177 (>1)	0.115 (>1)
Refinement statistics		
Resolution (Å)	42.7 – 4.0	63.3 – 3.3
R_{work} (%)	31.0	20.4
R_{free} (%)	35.9	25.8
Average B, all atoms (A^2)	166	130.0
Favored rotamers (%)	100	99
Ramachandran plot (%)		
Favored	96	98
Allowed	4	2

Table 2.

Non-normalized (nmol P/μg/min) and normalized (%) activity as well as the apparent Ca^{2+} affinity of the SERCA isoforms and chimeras. Mean values are given with standard deviation in parentheses. N=3 for each measurement.

	K_m (μM)	**V_{max} (nmol P/μg/min)**	**V_{max} (%)**	**n**
SERCA1a WT	0.19 ± 0.04	0.51 ± 0.17	100.9 ± 2.1	1.5 ± 0.1
SERCA1a-L7/8-2a	0.16 ± 0.04	0.28 ± 0.08	80.1 ± 2.5	1.5 ± 0.2
SERCA2a WT	0.14 ± 0.02	0.18 ± 0.06	100.0 ± 2.8	1.5 ± 0.1
SERCA2a-L7/8-1a	0.10 ± 0.02	0.13 ± 0.07	71.6 ± 4.9	1.5 ± 0.1

Supplementary

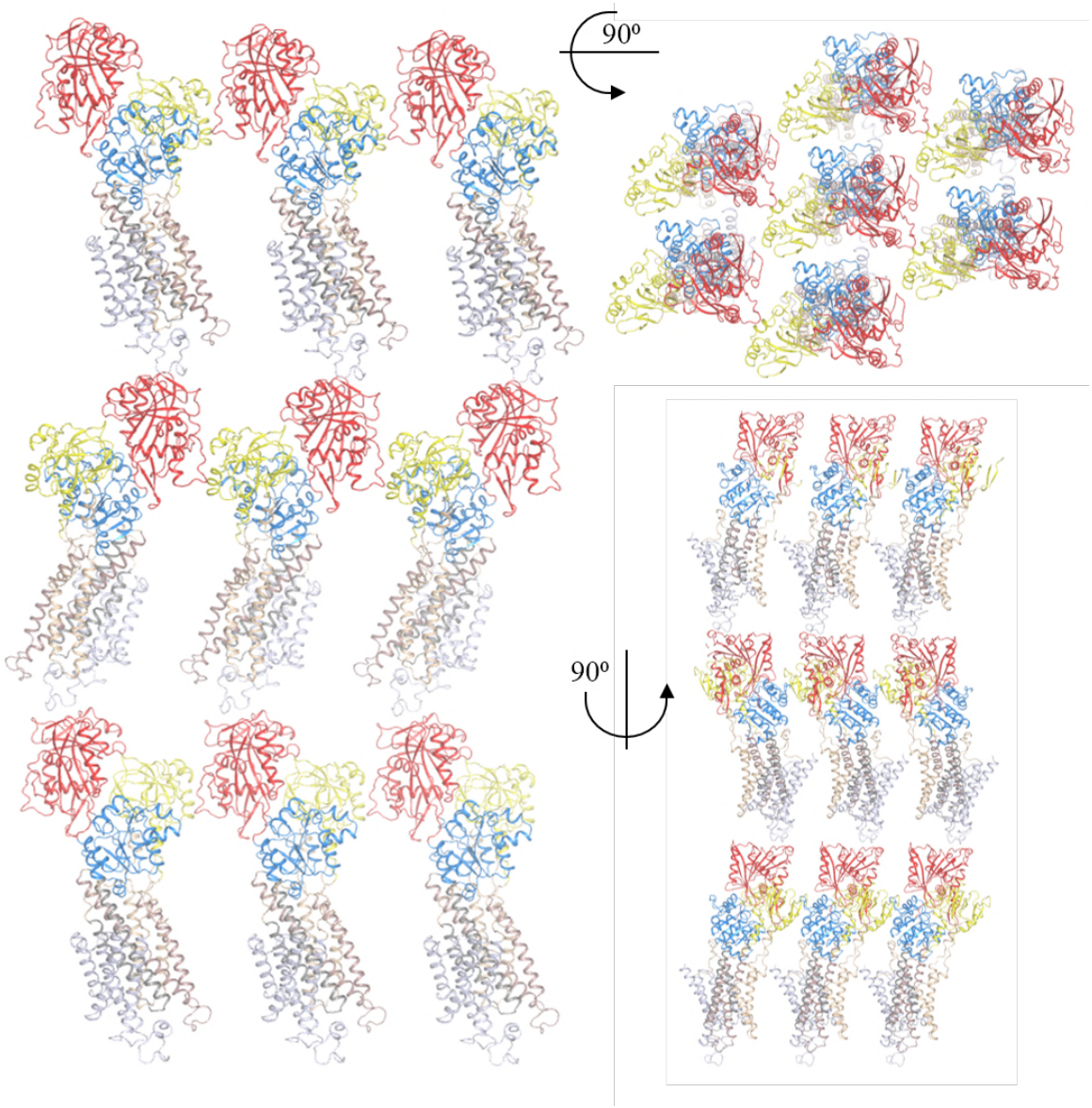

Supplementary Figure 1. Packing of SERCA2a E2-AlF_4^--CPA crystals

Parallel packing of the SERCA2a structure in the E2-AlF_4^--CPA conformational state. SERCA2a domains are colored the same as in Figure 2B and 3B. SERCA2a forms contact points between the A-domains and N-domains (Met1-Asn3, His15 to Glu458-Lys460) and between the A-domain (Arg134, Arg139, Lys141) and the P-domain (Glu659, Glu667, Ser663), as well as N-(Thr506-Ser509, Asp567-Arg571) domain and L7/8 (Asp859-Arg863, Lys876-Gly884).

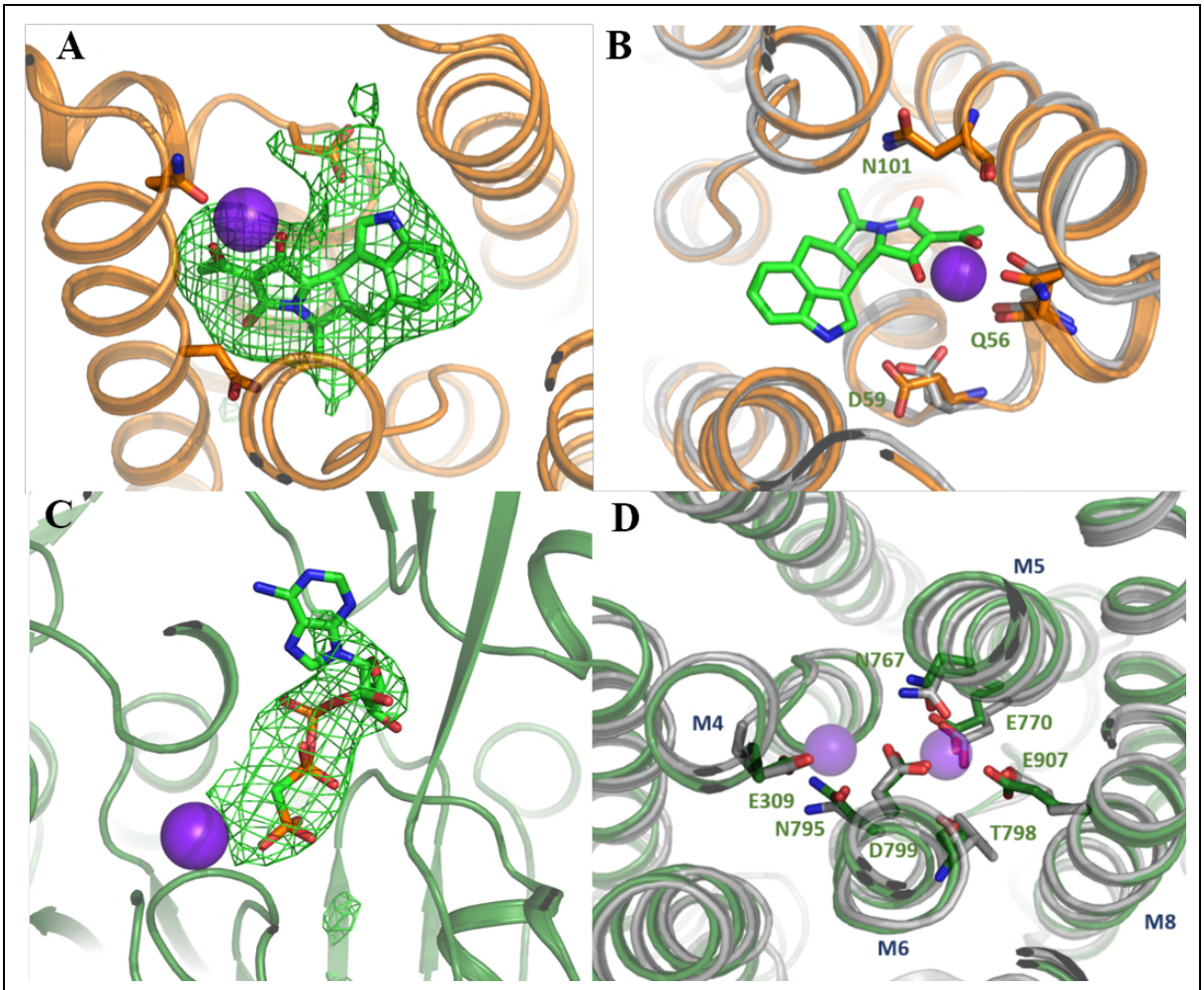

Supplementary Figure 2. Coordination of ions and molecules in the SERCA2a structures

Ca^{2+} ions are shown in purple spheres. Omit maps for the CPA (A) and the AMPPCP (C) molecules contoured at 3σ. B. CPA coordination in $[H_{2\text{-}3}]$E2-AlF_4^--CPA state of SERCA, SERCA1a is depicted in grey, SERCA2a in orange. D. coordination of Ca^{2+} ions in the $[Ca_2]$E1-AMPPCP state. SERCA1a is shown in grey, SERCA2a in green. Residues are marked according to the SERCA2a numbering.


rSERCA1a MEAAHSKSTE ECLAYFGVSE TTGLTPDQVK RHLEKYGHNE LPAEEGKSLW
pSERCA2a MENAHTKTVE EVLGHFGVNE STGLSLEQVK KLKERWGSNE LPAEEGKTLL
rSERCA1a ELVIEQFEDL LVRILLLAAC ISFVLAWFEE GEETITAFVE PFVILLILIA 100
pSERCA2a ELVIEQFEDL LVRILLLAAC ISFVLAWFEE GEETITAFVE PFVILLILVA 100
rSERCA1a NAIVGVWQER NAENAIEALK EYEPEMGKVY RADRKSVQRI KARDIVPGDI
pSERCA2a NAIVGVWQER NAENAIEALK EYEPEMGKVY RQDRKSVQRI KAKDIVPGDI
Ac
Ub
rSERCA1a VEVAVGDKVP ADIRILSIKS TTLRVDQSIL TGESVSVIKH TEPVPDPRAV 200
pSERCA2a VEIAVGDKVP ADIRLTSIKS TTLRVDQSIL TGESVSVIKH TDPVPDPRAV 200
Ub/Ac
rSERCA1a NQDKKNMLFS GTNIAAGKAL GIVATTGVST EIGKIRDQMA ATEQDKTPLQ
pSERCA2a NQDKKNMLFS GTNIAAGKAM GVVVATGVNT EIGKIRDEMV ATEQERTPLQ
Ac
Ac
Ac
rSERCA1a QKLDEFGEQL SKVISLICVA VWLINIGHFN DPVHGGSWIR GAIYYFKIAV 300
pSERCA2a QKLDEFGEQL SKVISLICIA VWIINIGHFN DPVHGGSWIR GAIYYFKIAV 300
rSERCA1a ALAVAAIPEG LPAVITTCLA LGTRRMAKKN AIVRSLPSVE TLGCTSVICS
pSERCA2a ALAVAAIPEG LPAVITTCLA LGTRRMAKKN AIVRSLPSVE TLGCTSVICS
rSERCA1a DKTGTLTTNQ MSVCKMFIID KVDGDFCSLN EFSITGSTYA PEGEVLKNDK 400
pSERCA2a DKTGTLTTNQ MSVCRMFILD KVEGDTCSLN EFTITGSTYA PIGEVHKDDK 400
Ac
Ac
rSERCA1a PIRSGQFDGL VELATICALC NDSSLDFNET KGVYEKVGEA TETALTTLVE
pSERCA2a PVKCHQYDGL VELATICALC NDSALDYNEA KGVYEKVGEA TETALTCLVE
P
Ac/Ub
rSERCA1a KMNVFNTEVR NLSKVERANA CNSVIRQLMK KEFTLEFSRD RKSMSVYCSP 500
pSERCA2a KMNVFDTELK GLSKIERANA CNSVIKQLMK KEFTLEFSRD RKSMSVYCTP 500
Ac
Ac
Ac
Ac
Ac/Ub
Ub
rSERCA1a AKSSRAAVGN KMFVKGAPEG VIDRCNYVRV GTTRVPMTGP VKEKILSVIK
pSERCA2a NKPSRTSM-S KMFVKGAPEG VIDRCTHIRV GSTKVPMTPG VKQKIMSVIR
Ac
Ac
Ac
rSERCA1a EWGTGRDTLR CLALATRDTP PKREEMVLDD SSRFMEYETD LTFVGVVGML 600
pSERCA2a EWGSGSDTLR CLALATHDNP MRREEMNLED SANFIKYETN LTFVGCVGML 599
rSERCA1a DPPRKEVMGS IQLCRDAGIR VIMITGDNKG TAIAICRRIG IFGENEEVAD
pSERCA2a DPPRIEVASS VKLCRQAGIR VIMITGDNKG TAVAICRRIG IFGQDEDVTS
Ac
rSERCA1a RAYTGREFDD LPLAEQREAC RRACCFARVE PSHKSKIVEY LQSYDEITAM 700
pSERCA2a KAFTGREFDE LNPSAQREAC LNARCFARVE PSHKSKIVEF LQSFDEITAM 699
P
P
Ac
rSERCA1a TGDGVNDAPA LKKAEIGIAM GSGTAVAKTA SEMVLADDNF STIVAAVEEG
pSERCA2a TGDGVNDAPA LKKSEIGIAM GSGTAVAKTA SEMVLADDNF STIVAAVEEG
Ac
Ac
rSERCA1a RAIYNNMKQF IRYLISSNVG EVVCIFLTAA LGLPEALIPV QLLWVNLVTD 800
pSERCA2a RAIYNNMKQF IRYLISSNVG EVVCIFLTAA LGFPEALIPV QLLWVNLVTD 799
Ac
rSERCA1a GLPATALGFN PPDLDIMDRP PRSPKEPLIS GWLFFRYMAI GGYVGAATVG
pSERCA2a GLPATALGFN PPDLDIMNKP PRNPKEPLIS GWLFFRYLAI GCYVGAATVG
rSERCA1a AAAWWFMYAE DGPGVTYHQL THFMQCTEDH PHFEGLDCEI FEAPEPMTMA 900
pSERCA2a AAAWWFIAAD GGPRVTFYQL SHFLQCKEDN PDFEGVDCAV FESPYPMTMA 899
rSERCA1a LSVLVTIEMC NALNSLSENQ SLMRMPPWVN IWLLGSICLS MSLHFLILYV
pSERCA2a LSVLVTIEMC NALNSLSENQ SLLRMPPWEN IWLVGSICLS MSLHFLILYV
rSERCA1a DPLPMIFKLK ALDLTQWLMV LKISLPVIGL DEILKFIARN YLEG---- 994
pSERCA2a EPLPLIFQIT PLNLTQWLMV LKISLPVILM DETLKFVARN YLEPAILE 997

Supplementary Figure 3. Sequence alignment of SERCA1a and SERCA2a

Alignment of rabbit SERCA1a and pig SERCA2a protein sequences indicating the eight most conserved regions in P-type ATPases (red squares) (Axelsen & Palmgren, 1998). The post-translational modifications found by MS in this study are marked by blue (reported before) and green squares (identified in this study).

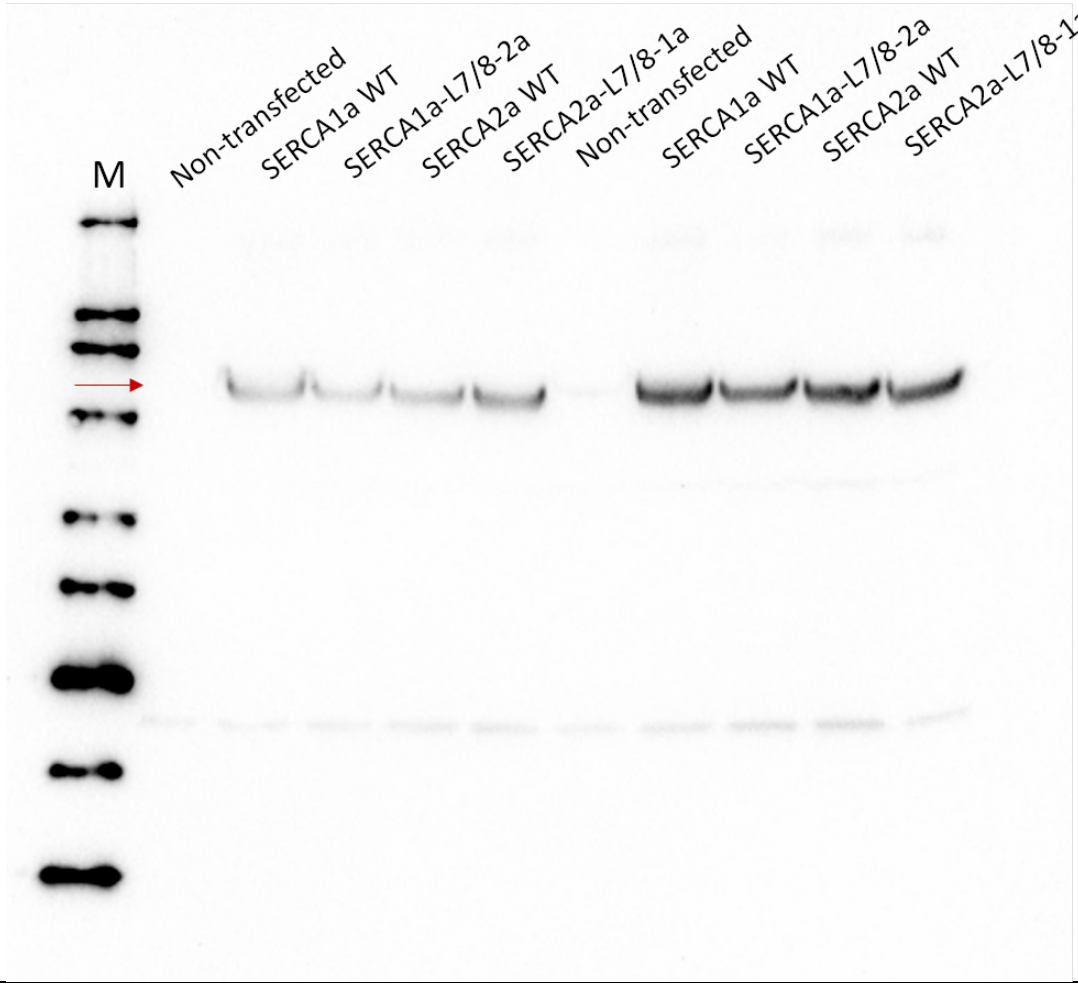

Supplementary Figure 4. Expression levels of SERCA1a and SERCA2a constructs

Immunoblot with a non-isoform specific SERCA TRY2 antibody (Mountian *et al*, 2001) depicting similar protein levels of the WT and chimera constructs of SERCA2a and SERCA1a following transient expression in COS cells.

Supplementary Table 1. Conservation of the SERCA1a and SERCA2a specific residues based on 68 and 83 vertebrate sequences, respectively. For SERCA1a, all of the distinct residues in rabbit SERCA1a and pig SERCA2a are at least 39% conserved and 79% are at least 70% conserved, 12.5%. For SERCA2a, all of the distinct residues are at least 43% conserved, while 89% are at least 70% conserved. Rabbit S1a RN – rabbit SERCA1a residue name, rabbit S1a RN – SERCA1a residue number, pig S2a RN – pig SERCA2a residue name, pig S2a RN – SERCA2a residue number.

Rabbit S1a RN	Rabbit S1a RN	Conservation (%)	Substitutions	Pig S2a RN	Pig S2a RN	Conservation (%)	Substitutions
Ala	3	70.1	A 70%; N 25%; Q 1%; S 1%	Asn	3	84.3	N 84%; R 1%; S 1%
Ser	6	43.3	S 43%; A 40%; T 12%; I 3%	Thr	6	83.1	T 83%; M 1%; R 1%; S 1%
Ser	8	70.1	T 70%; S 16%; E 10%; G 1%	Thr	8	77.1	T 77%; S 7%; N 1%; V 1%
Thr	9	79.1	T 79%; P 7%; V 6%; S 3%; A 1%; G 1%	Val	9	84.3	V 84%; G 1%; S 1%
Cys	12	94.0	C 94%; V 4%	Val	12	83.1	V 83%; M 1%; R 1%; S 1%; T 1%
Ala	14	86.6	A 87%; S 12%	Gly	14	59.0	G 59%; A 20%; S 6%; K 1%
Tyr	15	91.0	Y 91%; H 6%; F 1%	His	15	59.0	H 59%; Y 22%; A 1%; E 1%; G 1%; N 1%; S 1%
Ser	19	73.1	S 73%; N 19%; T 4%; D 1%	Asp	19	81.9	N 82%; D 1%; G 1%; K 1%; L 1%
Thr	21	68.7	T 69%; N 16%; S 4%; A 3%; D 3%; H 3%	Ser	21	84.3	S 84%; A 1%; E 1%; G 1%
Thr	25	61.2	T 61%; S 37%	Ser	25	80.7	S 81%; G 4%; D 1%; T 1%; V 1%
Pro	26	86.6	P 87%; Q 7%; E 1%; G 1%; L 1%	Leu	26	83.1	L 83%; V 2%; P 1%; X 1%
Asp	27	74.6	D 75%; E 22%; P 1%	Glu	27	75.9	E 76%; D 6%; P 2%; Q 2%; T 1%
Arg	31	77.6	R 78%; K 19%; L 3%	Lys	31	78.3	K 78%; R 6%; A 1%; H 1%; I 1%
His	32	53.7	H 54%; N 37%; S 7%; A 1%	Leu	32	74.7	L 75%; Q 7%; M 2%; N 2%; R 1%
Leu	33	82.1	L 82%; F 13%; Q 3%; I 1%	Lys	33	81.9	K 82%; Q 2%; E 1%; L 1%; R 1%
Lys	35	95.5	K 96%; S 3%; R 1%	Arg	35	60.2	R 60%; K 27%; Q 1%
Tyr	36	83.6	Y 84%; F 15%; H 1%	Trp	36	84.3	W 84%; F 1%; Y 1%
His	38	65.7	P 66%; H 18%; F 6%; Y 6%; W 3%; L 1%	Ser	38	79.5	S 80%; A 4%; L 4%; P 1%; T 1%
Ser	48	77.6	S 78%; T 22%	Thr	48	84.3	T 84%; S 10%; P 1%
Trp	50	100	W 100%	Leu	50	83.1	L 83%; W 12%
Ile	99	98.5	I 99%; L 1%	Val	99	88.0	V 88%; I 10%
Ala	132	73.1	A 73%; S 25%; G 1%	Gln	132	96.4	Q 96%; E 1%
Arg	143	97.0	R 97%; S 3%	Lys	143	72.3	K 72%; R 25%
Val	153	92.5	V 93%; I 4%; S 1%; W 1%	Ile	153	66.3	I 66%; V 33%

Ile	165	88.1	I 88%; L 10%; S 1%	Leu	165	71.1	L 71%; I 25%
Leu	166	71.6	L 72%; I 15%; T 6%; V 6%; S 1%	Thr	166	90.4	T 90%; S 4%; C 2%
Glu	192	55.2	E 55%; D 45%	Asp	192	98.8	D 99%; E 1%
Leu	220	47.8	L 48%; I 30%; V 19%; T 3%	Met	220	86.7	M 87%; I 10%; V 4%
Ile	222	79.1	I 79%; V 21%	Val	222	98.8	V 99%; I 1%
Ala	224	67.2	A 67%; V 19%; I 13%	Val	224	83.1	V 83%; I 16%; L 1%
Thr	225	62.7	T 63%; A 36%; S 1%	Ala	225	97.6	A 98%; G 1%; N 1%
Ser	229	50.7	S 51%; N 30%; G 15%; T 3%; A 1%	Asn	229	97.6	N 98%; F 1%; G 1%
Gln	238	82.1	Q 82%; E 18%	Glu	238	98.8	E 99%; N 1%
Ala	240	98.5	A 99%; V 1%	Val	240	89.2	V 89%; A 10%; K 1%
Asp	245	68.7	D 69%; E 31%	Glu	245	98.8	E 99%; D 1%
Lys	246	100	K 100%	Arg	246	91.6	R 92%; K 7%; L 1%
Val	269	100	V 100%	Ile	269	100.0	I 100%
Leu	273	92.5	L 93%; A 3%; I 3%; M 1%	Ile	273	91.6	I 92%; M 6%; A 1%; L 1%
Lys	365	89.6	K 90%; R 10%	Arg	365	98.8	R 99%; K 1%
Ile	369	64.2	I 64%; V 21%; L 12%; Q 1%; Y 1%	Leu	369	89.2	L 89%; V 8%; I 1%
Asp	373	65.7	D 66%; E 30%; G 1%; H 1%; K 1%	Glu	373	91.6	E 92%; D 6%; R 1%; S 1%
Phe	376	43.3	I 43%; L 15%; V 10%; F 9%; N 6%; S 6%; H 3%; M 3%; Q 1%; T 1%; Y 1%	Thr	376	56.6	T 57%; S 34%; N 6%; A 1%; Q 1%
Ser	383	74.6	S 75%; D 13%; T 7%; A 3%; V 1%	Thr	383	91.6	T 92%; N 4%; S 2%; D 1%; I 1%
Glu	392	97.0	E 97%; G 3%	Ile	392	62.7	I 63%; M 23%; E 8%; L 2%; V 2%; T 1%
Leu	396	74.6	L 75%; T 10%; M 7%; Q 4%; S 3%	His	396	83.1	H 83%; Y 5%; L 4%; Q 4%; F 2%; C 1%; T 1%
Asn	398	94.0	N 94%; G 3%; S 3%	Asp	398	97.6	D 98%; E 1%; N 1%
Ile	402	79.1	V 79%; I 16%; T 4%	Val	402	79.5	V 80%; I 19%
Arg	403	73.1	R 73%; K 24%; N 3%	Lys	403	88.0	K 88%; N 6%; R 4%; V 1%
Ser	404	47.8	A 48%; S 19%; P 18%; C 15%	Cys	404	95.2	C 95%; S 2%; E 1%
Gly	405	97.0	G 97%; S 3%	His	405	69.9	H 70%; S 24%; T 2%; E 1%; K 1%
Phe	407	92.5	Y 93%; F 6%; H 1%	Tyr	407	94.0	Y 94%; N 2%; F 1%; H 1%
Ser	424	94.0	S 94%; A 6%	Ala	424	69.9	A 70%; S 30%
Phe	427	79.1	F 79%; Y 21%	Tyr	427	89.2	Y 89%; F 11%

Thr	430	38.8	A 39%; T 33%; S 27%; N 1%	Ala	430	92.8	A 93%; T 4%; V 2%; S 1%
Thr	447	77.6	T 78%; C 22%	Cys	447	98.8	C 99%; V 1%
Asn	456	98.5	N 99%; S 1%	Asp	456	98.8	D 99%; E 1%
Val	459	100	V 100%	Leu	459	94.0	L 94%; V 4%; I 2%
Arg	460	91.0	R 91%; K 9%	Lys	460	96.4	K 96%; A 2%; R 1%
Asn	461	61.2	S 61%; N 24%; G 15%	Gly	461	95.2	G 95%; N 2%; S 2%
Val	465	97.0	V 97%; I 1%; P 1%	Ile	465	97.6	I 98%; S 1%; V 1%
Arg	476	68.7	R 69%; K 31%	Lys	476	94.0	K 94%; T 2%; H 1%; R 1%; S 1%
Ser	499	80.6	S 81%; T 18%; I 1%	Thr	499	95.2	T 95%; S 4%; I 1%
Ala	501	97.0	A 97%; S 3%	Asn	501	96.4	N 96%; K 2%; A 1%
Ser	503	52.2	S 52%; A 21%; G 3%; P 3%	Pro	503	90.4	P 90%; S 2%; N 1%
Ala	506	97.0	A 97%	Thr	506	92.8	T 93%; S 4%; R 2%; H 1%
Ala	507	83.6	A 84%; P 6%; S 4%; V 3%	Ser	507	97.6	S 98%; A 2%
Val	508	94.0	V 94%; L 3%	Met	508	92.8	M 93%; A 2%; L 2%; H 1%; S 1%
Gly	509	100	G 100%				
Asn	510	94.0	N 94%; A 3%; S 3%	Ser	509	88.0	S 88%; A 5%; G 5%; N 1%; P 1%
Asn	526	85.1	N 85%; A 10%; S 3%; T 1%	Thr	525	97.6	T 98%; A 1%; N 1%
Tyr	527	100	Y 100%	His	526	95.2	H 95%; Y 4%; F 1%
Val	528	100	V 100%	Ile	527	72.3	I 72%; V 28%
Thr	532	97.0	T 97%; S 3%	Ser	531	78.3	S 78%; N 17%; T 2%; G 1%; K 1%
Arg	534	100	R 100%	Lys	533	97.6	K 98%; R 2%
Gly	539	73.1	G 73%; S 12%; P 10%; E 1%; N 1%; T 1%	Pro	538	55.4	P 55%; S 31%; A 8%; Q 4%; K 1%
Pro	540	74.6	P 75%; A 12%; S 6%; V 4%; G 1%; N 1%	Gly	539	96.4	G 96%; A 2%; Q 1%
Glu	543	67.2	E 67%; D 31%; N 1%	Gln	542	90.4	Q 90%; E 6%; H 2%; D 1%
Leu	546	64.2	M 64%; L 34%; N 1%	Met	545	98.8	M 99%; L 1%
Lys	550	98.5	K 99%; R 1%	Arg	549	98.8	R 99%; N 1%
Thr	554	100	T 100%	Ser	553	69.9	S 70%; T 30%
Arg	556	98.5	R 99%; Q 1%	Ser	555	65.1	S 65%; R 31%; N 2%; K 1%
Arg	567	100	R 100%	His	566	90.4	H 90%; R 8%; V 1%

Thr	569	88.1	T 88%; S 6%; A 3%; N 3%	Asn	568	95.2	N 95%; A 2%; D 1%; S 1%
Pro	571	89.6	P 90%; L 10%	Met	570	62.7	L 63%; P 31%; M 4%; A 1%; I 1%
Lys	572	88.1	K 88%; R 12%	Arg	571	84.3	R 84%; K 14%; S 1%
Val	577	44.8	V 45%; I 36%; N 12%; K 3%; F 1%; M 1%; S 1%	Asn	576	43.4	N 43%; H 42%; V 6%; K 4%; Y 2%; D 1%; Q 1%
Asp	579	70.1	D 70%; E 28%; V 1%	Glu	578	89.2	E 89%; S 4%; D 2%; V 2%; K 1%; T 1%
Ser	582	47.8	A 48%; T 36%; S 13%; N 3%	Ala	581	78.3	A 78%; S 14%; T 4%; K 1%; N 1%; V 1%
Arg	583	52.2	K 52%; R 45%; H 3%	Asn	582	90.4	N 90%; K 5%; R 4%; S 1%
Met	585	47.8	M 48%; L 18%; A 13%; V 10%; I 7%; G 3%	Ile	584	91.6	I 92%; A 6%; V 2%
Glu	586	76.1	E 76%; D 24%	Lys	585	71.1	K 71%; N 17%; E 5%; G 2%; T 2%; D 1%; S 1%
Asp	590	100	D 100%	Asn	589	91.6	N 92%; D 6%; G 2%
Val	596	68.7	V 69%; C 31%	Cys	595	98.8	C 99%; V 1%
Lys	605	100	K 100%	Ile	604	77.1	I 77%; T 19%; Q 2%; S 1%
Met	608	56.7	T 57%; M 39%; V 3%; I 1%	Ala	607	98.8	A 99%; R 1%
Gly	609	94.0	G 94%; S 4%; D 1%	Ser	608	88.0	S 88%; A 11%; D 1%
Ile	611	100	I 100%	Val	610	67.5	V 67%; I 33%
Gln	612	74.6	Q 75%; E 16%; K 7%; R 1%	Lys	611	97.6	K 98%; M 2%
Asp	616	80.6	D 81%; A 12%; E 7%	Gln	615	92.8	Q 93%; L 5%; E 1%; H 1%
Ile	633	89.6	I 90%; V 10%	Val	632	97.6	V 98%; E 1%
Glu	644	97.0	E 97%; D 3%	Gln	643	59.0	Q 59%; E 29%; L 4%; S 2%; D 1%; H 1%; N 1%
Asn	645	59.7	N 60%; D 15%; S 15%; E 10%	Asp	644	81.9	D 82%; E 14%; N 1%
Glu	647	64.2	E 64%; D 31%; Q 4%	Asp	646	94.0	D 94%; E 2%; S 1%
Ala	649	44.8	A 45%; T 40%; S 12%; V 3%	Thr	648	59.0	T 59%; S 28%; D 5%; A 4%; H 1%; N 1%; V 1%
Asp	650	65.7	D 66%; G 24%; R 4%; E 1%; N 1%; S 1%; T 1%	Ser	649	56.6	S 57%; T 17%; A 11%; K 5%; F 2%; C 1%; D 1%; E 1%; G 1%; L 1%; R 1%
Arg	651	88.1	R 88%; K 6%; C 3%; L 3%	Lys	650	88.0	K 88%; M 6%; L 2%; R 2%
Tyr	653	83.6	Y 84%; F 16%	Phe	652	97.6	F 98%; W 1%
Asp	660	100	D 100%	Glu	659	95.2	E 95%; D 4%; G 1%
Pro	662	97.0	P 97%; S 3%	Asn	661	69.9	S 70%; N 27%; A 2%; G 1%
Leu	663	79.1	L 79%; P 16%; S 3%; M 1%	Pro	662	81.9	P 82%; L 16%; E 1%; V 1%

Ala	664	61.2	A 61%; P 19%; T 6%; G 3%; H 3%; Y 3%; Q 1%; S 1%; V 1%	Ser	663	63.9	S 64%; A 23%; P 6%; Q 5%; H 1%; V 1%
Glu	665	92.5	E 93%; Q 6%; D 1%	Ala	664	96.4	A 96%; E 2%; F 1%
Arg	671	89.6	R 90%; K 10%	Leu	670	74.7	L 75%; H 14%; T 6%; M 2%; R 1%; W 1%
Arg	672	86.6	R 87%; K 10%; H 3%	Asn	671	78.3	N 78%; H 18%; D 1%; T 1%; V 1%
Cys	674	89.6	C 90%; S 9%; R 1%	Arg	673	98.8	R 99%; S 1%
Tyr	690	65.7	Y 66%; F 34%	Phe	689	95.2	F 95%; Y 5%
Tyr	694	49.3	F 49%; Y 46%; C 3%; N 1%	Phe	693	94.0	F 94%; M 2%; D 1%; L 1%; S 1%
Ala	714	100	A 100%	Ser	713	61.4	A 61%; S 39%
Leu	783	98.5	L 99%	Phe	782	97.6	F 98%; M 2%
Asp	818	83.6	D 84%; G 13%; N 1%	Asn	817	92.8	N 93%; D 2%; E 2%; K 1%; S 1%
Arg	819	76.1	R 76%; K 21%	Lys	818	98.8	K 99%
Ser	823	91.0	S 91%; T 7%	Asn	822	94.0	N 94%; S 4%; R 1%
Met	838	73.1	M 73%; L 27%	Leu	837	98.8	L 99%; V 1%
Gly	842	95.5	G 96%; A 3%	Cys	841	96.4	C 96%; G 2%; V 1%
Met	857	65.7	L 66%; M 27%; I 6%	Ile	856	91.6	I 92%; V 4%; T 2%; M 1%
Tyr	858	97.0	Y 97%; F 1%	Ala	857	94.0	A 94%; L 2%; F 1%; V 1%
Glu	860	56.7	E 57%; D 39%; P 1%; S 1%	Asp	859	85.5	D 86%; E 13%
Asp	861	86.6	D 87%; E 9%; T 3%	Gly	860	86.7	G 87%; D 11%; E 1%
Gly	864	62.7	H 63%; G 12%; M 9%; E 4%; N 4%; S 4%; A 1%; Q 1%	Arg	863	88.0	R 88%; K 4%; M 4%; Q 4%
Tyr	867	79.1	Y 79%; F 19%; L 1%	Phe	866	90.4	F 90%; L 7%; Y 2%
His	868	49.3	S 49%; Y 30%; H 13%; N 6%; Q 1%	Tyr	867	98.8	Y 99%; S 1%
Thr	871	70.1	T 70%; S 30%	Ser	870	100.0	S 100%
Met	874	100	M 100%	Leu	873	98.8	L 99%; M 1%
Thr	877	71.6	T 72%; S 10%; N 9%; H 4%; G 3%; A 1%	Lys	876	90.4	K 90%; S 5%; A 2%; R 2%
His	880	91.0	N 91%; H 4%; S 4%	Asn	879	98.8	N 99%; S 1%
His	882	58.2	D 58%; H 22%; E 16%; N 3%	Asp	881	94.0	D 94%; E 5%; H 1%
Leu	886	43.3	V 43%; L 31%; I 18%; H 4%; M 3%	Val	885	91.6	V 92%; L 7%; I 1%
Glu	889	97.0	E 97%; D 3%	Ala	888	66.3	A 66%; V 16%; H 6%; E 5%; L 5%; G 1%; N 1%

Ile	890	61.2	V 61%; I 39%	Val	889	57.8	I 58%; V 42%
Ala	893	76.1	A 76%; S 24%	Ser	892	98.8	S 99%; D 1%
Glu	895	61.2	E 61%; V 16%; P 12%; Q 7%; F 1%; T 1%	Tyr	894	98.8	Y 99%; H 1%
Met	923	49.3	L 49%; V 22%; M 16%; I 12%	Leu	922	80.7	L 81%; M 18%; V 1%
Val	929	83.6	V 84%; S 16%	Glu	928	98.8	E 99%; K 1%
Leu	934	67.2	L 67%; V 21%; M 9%; A 3%	Val	933	84.3	V 84%; L 14%; M 1%
Asp	951	88.1	D 88%; E 12%	Glu	950	98.8	E 99%; P 1%
Met	955	100	M 100%	Leu	954	77.1	L 77%; I 16%; V 6%; P 1%
Lys	958	100	K 100%	Gln	957	98.8	Q 99%; R 1%
Leu	959	100	L 100%	Ile	958	98.8	I 99%; V 1%
Lys	960	41.8	R 42%; T 31%; Q 22%; K 3%; E 1%	Thr	959	100.0	T 100%
Ala	961	67.2	A 67%; H 16%; P 16%	Pro	960	100.0	P 100%
Asp	963	73.1	D 73%; N 21%; T 4%; S 1%	Asn	962	95.2	N 95%; D 5%
Gly	979	65.7	G 66%; L 33%; A 1%	Leu	978	98.8	L 99%; F 1%
Leu	980	83.6	L 84%; I 16%	Met	979	65.1	M 65%; L 34%; I 1%
Ile	983	44.8	I 45%; L 33%; V 18%; A 4%	Thr	982	92.8	T 93%; L 6%; I 1%
Ile	987	49.3	V 49%; I 48%; A 1%; F 1%	Val	986	92.8	V 93%; A 4%; F 2%; I 1%
Gly	994	53.7	G 54%; D 22%; A 9%; E 3%; Q 3%; V 3%; C 1%; P 1%; T 1%	Pro	993	95.2	P 95%; F 2%; Q 1%; S 1%
				Ala	994	71.1	G 71%; A 24%; V 2%; E 1%; S 1%

Supplementary Table 2. A list of PTMs found in the MS analysis of purified SERCA1a and SERCA2a. Only peptides expressing a high identification confidence and a localization confidence of 99%+ were chosen and are shown in this table. PTMs that have not been previously reported elsewhere are highlighted in bold. PTMs that were found alternatively modified either in this study or elsewhere are indicated with (+). The species where the previously reported PTMs were identified are also indicated (H – humans, R – rats, M – mice, GP – guinea pig). In SERCA1a either Lys 204 or Lys 205 is ubiquitinated (*).

PTMs found in this study for rabbit SERCA1a and pig SERCA2a

Res	Isoform	Modification found	Species this PTM was also reported in	Alternative PTM reported	Reference for this PTM in other species
Lys 205	**SERCA1a**	**acetylation (+)**			
Lys 492	SERCA1a	acetylation	H	ubiquitination	(Hornbeck *et al*, 2015)
Lys 511	SERCA1a	acetylation **(+)**	R	ubiquitination	(Lundby *et al*, 2012a)
Lys 515	SERCA1a	acetylation **(+)**	H+R	ubiquitination	(Wu *et al*, 2015; Lundby *et al*, 2012a)
Lys 572	SERCA1a	acetylation **(+)**	R	ubiquitination	(Lundby *et al*, 2012a)
Lys 713	**SERCA1a**	**acetylation (+)**		ubiquitination	
Lys 169	SERCA1a	ubiquitination	M		(Wagner *et al*, 2012)
Lys 204/ Lys 205*	**SERCA1a**	**ubiquitination (+)**			
Lys 492	SERCA1a	ubiquitination	M	acetylation	(Wagner *et al*, 2012; Hornbeck *et al*, 2015)
Lys 515	SERCA1a	ubiquitination **(+)**	H+M	acetylation	(Wagner *et al*, 2012; Kim *et al*, 2011; Hornbeck *et al*, 2015)
Lys 542	SERCA1a	ubiquitination	M	acetylation	(Wagner *et al*, 2012)
Ser473	SERCA1a	phosphorylation	H		(Mertins *et al*, 2013; Zhao *et al*, 2011)
Lys 128	**SERCA2a**	**acetylation**		ubiquitination	
Lys 205	**SERCA2a**	**acetylation (+)**			

Lys 218	SERCA2a	acetylation **(+)**	H		(Hornbeck *et al*, 2015)
Lys 234	**SERCA2a**	**acetylation**			
Lys 352	**SERCA2a**	**acetylation**			
Lys 371	**SERCA2a**	**acetylation**			
Lys 451	**SERCA2a**	**acetylation**		ubiquitination	
Lys 476	SERCA2a	acetylation	H	ubiquitination	(Wu *et al*, 2015)
Lys 492	**SERCA2a**	**acetylation**		ubiquitination	
Lys 514	SERCA2a	acetylation	H+R	ubiquitination	(Wu *et al*, 2015; Lundby *et al*, 2012a)
Lys 533	SERCA2a	acetylation	GP	ubiquitination	(Foster *et al*, 2013)
Lys 628	**SERCA2a**	**acetylation**		ubiquitination	
Lys 712	**SERCA2a**	**acetylation**		ubiquitination	
Lys 727	**SERCA2a**	**acetylation**			
Lys 757	**SERCA2a**	**acetylation**		ubiquitination	
Ser 663	SERCA2a	phosphorylation	H+M+R		(Hornbeck *et al*, 2015) and references therein
Ser 692	SERCA2a	phosphorylation	H		(Lundby *et al*, 2012b)

Supplementary Table 3. Salt bridges found during MD simulations. Only unique interactions of SERCA1a and SERCA2a present during at least 10% of the total simulation time are shown. Residue pairs that form salt bridges in both isoforms but have a different interaction time of at least 20% are also shown below. AA1 and AA2 stand for the first and second amino acids in the interacting residue pair, IS – isoform specific, % - percent of total simulation time spent interacting.

		%	**AA1**		**AA2**		**AA1_IS**	**Loop**	**AA2_IS**	**Loop**
SERCA1a	668E-671R	100	668	E	671	R			Yes	
	879D-882H	99.2	879	D	882	H		L7/8	Yes	L7/8
	924R-982E	94.81	924	R	982	E				
	38H-40E	92.08	38	H	40	E	Yes			
	668E-672R	91.82	668	E	672	R			Yes	
	583R-586E	87.13	583	R	586	E	Yes		Yes	
	83E-958K	80.2	83	E	958	K			Yes	L9/10

	580D-583R	79.21	580	D	583	R			Yes	
	556R-644E	66.34	556	R	644	E	Yes		Yes	
	604R-606E	58.42	604	R	606	E				
	650D-651R	58.42	650	D	651	R	Yes		Yes	
	892E-958K	56.49	892	E	958	K		L7/8	Yes	L9/10
	895E-960K	49.7	895	E	960	K	Yes	L7/8	Yes	L9/10
	234K-680E	48.7	234	K	680	E				
	665E-672R	39.52	665	E	672	R	Yes		Yes	
	290R-878E	32.14	290	R	878	E		L3/4		L7/8
	556R-557D	26.73	556	R	557	D	Yes			
	605K-606E	22.77	605	K	606	E	Yes			
	567R-586E	19.8	567	R	586	E	Yes		Yes	
	650D-672R	17.82	650	D	672	R	Yes		Yes	
	524R-590D	15.84	524	R	590	D			Yes	
	152E-169K	14.85	152	E	169	K				
	822R-826E	13.86	822	R	826	E				
	868H-884E	13.37	868	H	884	E	Yes	L7/8		L7/8
	252K-826E	11.88	252	K	826	E				
	125E-139R	10.38	125	E	139	R				

		%	AA1		AA2		AA1_IS	Loop	AA2_IS	Loop
SERCA2a	234K-238E	93.07	234	K	238	E			Yes	
	645E-673R	92.08	645	E	673	R			Yes	
	11E-15H	87.13	11	E	15	H			Yes	
	80E-290R	57.09	80	E	290	R				L3/4
	398D-400K	55.89	398	D	400	K	Yes			
	33K-144D	54.46	33	K	144	D	Yes			
	79E-297K	54.46	79	E	297	K				
	403K-456D	49.7	403	K	456	D	Yes		Yes	
	394E-396H	45.54	394	E	396	H			Yes	
	761R-825E	43.51	761	R	825	E				
	183E-559R	29.7	183	E	559	R				
	566H-567D	29.7	566	H	567	D	Yes			

			711K-731E	29.7	711	K	731	E			
			243E-711K	22.77	243	E	711	K			
			365R-550E	20.79	365	R	550	E	Yes		
			614R-645E	19.56	614	R	645	E			
			284H-877E	18.56	284	H	877	E		L3/4	
			79E-290R	16.97	79	E	290	R			L3/4
Difference (%)	**SERCA2a**	**%**	**SERCA1a**	**%**							
96.41	58E-63R	99	58E-63R	2.59	58	E	63	R			
84.23	450E-467R	15.77	450E-467R	100	450	E	467	R			
76.05	297K-784E	4.39	297K-785E	80.44	297	K	785	E			L5/6
75.85	408D-528R	76.05	408D-529R	0.2	408	D	529	R			
74.85	636R-645E	25.15	637R-646E	100	637	R	646	E			
72.65	528R-567D	21.16	529R-568D	93.81	529	R	568	D			
72.25	757K-917E	89.42	758K-918E	17.17	758	K	918	E			
71.65	412E-510K	73.65	412E-511K	2	412	E	511	K			
66.26	352K-600D	93.41	352K-601D	27.15	352	K	601	D			
63.07	351D-352K	7.39	351D-352K	70.46	351	D	352	K			
59.28	603R-605E	0.2	604R-606E	59.48	604	R	606	E			
58.42	645E-650K	33.66	646E-651R	92.08	646	E	651	R		Yes	
53.9	412E-528R	38.52	412E-529R	92.42	412	E	529	R			
53.69	365R-381E	93.21	365K-381E	39.52	365	K	381	E	Yes		
52.9	278H-281D	9.38	278H-281D	62.28	278	H	281	D		L3/4	L3/4
51.9	79E-297K	52.1	79E-297K	0.2	79	E	297	K			
51.5	658D-682H	14.57	659D-683H	66.07	659	D	683	H			
50.1	458E-460K	43.71	458E-460R	93.81	458	E	460	R		Yes	
50.1	761R-917E	28.14	762R-918E	78.24	762	R	918	E			
48.7	198R-658D	47.31	198R-659D	96.01	198	R	659	D			
46.53	40E-143K	51.49	40E-143R	98.02	40	E	143	R		Yes	
44.71	245E-246R	4.79	245D-246K	49.5	245	D	246	K	Yes	Yes	
43.31	109E-246R	88.62	109E-246K	45.31	109	E	246	K		Yes	
41.58	510K-567D	45.54	511K-568D	3.96	511	K	568	D			
39.92	628K-656E	50.9	629K-657E	10.98	629	K	657	E			
39.92	835R-917E	40.52	836R-918E	0.6	836	R	918	E			
36.53	198R-659E	41.32	198R-660D	4.79	198	R	660	D		Yes	

33.66	30K-34E	57.43	30K-34E	91.09	30	K	34	E				
32.73	243E-712K	2.2	243E-713K	34.93	243	E	713	K				
32.34	47K-55E	28.14	47K-55E	60.48	47	K	55	E				
30.7	174R-439E	48.51	174R-439E	79.21	174	R	439	E				
29.74	711K-731E	30.14	712K-732E	0.4	712	K	732	E				
29.71	2E-7K	25.74	2E-7K	55.45	2	E	7	K				
29.7	20E-169K	31.68	20E-169K	1.98	20	E	169	K				
29.14	183E-559R	29.54	183E-560R	0.4	183	E	560	R				
26.74	133D-134R	65.35	133D-134R	38.61	133	D	134	R				
25.74	113E-334R	90.1	113E-334R	64.36	113	E	334	R				
25.55	121E-158K	31.94	121E-158K	6.39	121	E	158	K				
20.79	619R-695E	82.18	620R-696E	61.39	620	R	696	E				
20.55	365R-556D	27.54	365K-557D	6.99	365	K	557	D	Yes			